“It is our choices, Harry, that show what we truly are, far more than our abilities.”

-Albus Dumbledore

Revealing the architecture and composition of the sperm flagellum tip

Doctoral Thesis

Davide Zabeo

Abstract

The eukaryotic flagellum is a membrane-bound protruding organelle with a cytoskeleton of microtubules. Flagella are found in unicellular as well as multicellular organisms, performing a variety of functions. Motile flagella enable cell locomotion, like in protists or spermatozoa, but can also create flows of fluids or mucus, like in respiratory airways. Flagella also act as cellular “antennas”, as their surface can probe the environment with sensorial receptors. The flagellar ultrastructure is often regarded as widely conserved among eukaryotes, however significant differences have been reported for the structure of the distal flagellar tip between organisms. The tip is where the flagellum grows and where intra-flagellar transport must unload and load cargo, making it a hub of flagellar-specific processes that are still relatively under-explored.

In humans, genetic mutations that impair proper flagellar function cause primary ciliary dyskinesia, a collective term for numerous pathologies which are still not fully characterized. To elucidate the ultrastructure of the human flagellar tip, we performed cryo-electron tomography on intact spermatozoa, plunge-frozen in their native environment. The results revealed drastic differences compared to commonly studied model organisms (**Paper I**). Additionally, a novel extensive structure (named TAILS) was discovered decorating the lumen of sperm tip microtubules (**Paper II**). These results together highlight the power of cryo-electron tomography in displaying complex cellular structures in their native environment, as well as the importance of studying the human system directly.

Lastly, a multi-pronged approach was designed to biochemically identify and characterize TAILS, based on a reverse structural biology perspective (**Paper III**). This included obtaining high-resolution structures of TAILS produced with different cryo-electron microscopy techniques, the first ever flagellar tip proteome and an evolutionary overview of TAILS conservation.

Publications

Here is the list of research papers that are included in this thesis.

PAPER I. **Davide Zabeo**, Jacob T Croft, Johanna L Höög. *Axonemal doublet microtubules can split into two complete singlets in human sperm flagellum tips*. FEBS Lett, 593: 892-902 (2019). https://doi.org/10.1002/1873-3468.13379

PAPER II. **Davide Zabeo**, John M Heumann, Cindi L Schwartz, Azusa Suzuki-Shinjo, Garry Morgan, Per O Widlund, Johanna L Höög. *A luminal interrupted helix in human sperm tail microtubules*. Sci Rep, 8, 2727 (2018). https://doi.org/10.1038/s41598-018-21165-8

PAPER III. Jacob T Croft*, **Davide Zabeo***, Vajradhar Acharya, Václav Bočan, Mandy Rettel, Matthew C Johnson, Frank Stein, Christer Edvardsson, Lenka Libusová, Mikhail Savitski, Per O Widlund, Radhika Subramanian, Justin M Kollman, Johanna L Höög.
*These authors contributed equally to the manuscript.
Identification and biochemical characterization of TAILS: a microtubule inner complex. Unpublished manuscript (2021).

Here is a list of other papers which I co-authored during my doctoral studies, but which are not included in this thesis.

PAPER IV. Jacob T Croft, **Davide Zabeo**, Radhika Subramanian, Johanna L Höög. *Composition, structure and function of the eukaryotic flagellum distal tip*. Essays Biochem, 62 (6): 815–828 (2018). https://doi.org/10.1042/EBC20180032

PAPER V. **Davide Zabeo**, Aleksander Cvjetkovic, Cecilia Lässer, Martin Schorb, Jan Lötvall & Johanna L Höög. *Exosomes purified from a single cell type have diverse morphology*. Journal of Extracellular Vesicles, 6:1 (2017). https://doi.org/10.1080/20013078.2017.1329476

PAPER VI. Aleksander Cvjetkovic, Rossella Crescitelli, Cecilia Lässer, **Davide Zabeo**, Per O Widlund, Thomas Nyström, Johanna L Höög, Jan Lötvall. *Extracellular vesicles in motion.* Matters (2017). https://doi.org/10.19185/matters.201704000003

PAPER VII. **Davide Zabeo**, Rossella Crescitelli, Eileen T O'Toole, Helio Roque, Johanna L Höög. *3D ultrastructure of multi-vesicular bodies in fission yeast*. Matters (2017). https://doi.org/10.19185/matters.201702000007

Contribution report

PAPER I. I contributed to the bovine sample preparation and cryo-EM. I calculated cryo-electron tomograms and analysed all the data. I wrote most of the manuscript and produced the figures.

PAPER II. I calculated cryo-electron tomograms and analysed most of the data. I performed sub-tomogram averaging of the TAILS-like density in doublet microtubules. I contributed to the writing of the manuscript and the production of the figures.

PAPER III. I led the project together with JTC under JLH's supervision. I contributed to the experimental design and project management. I was involved in the collection of the sperm samples from different species, their preparation for cryo-EM and data acquisition at SciLifeLab. I designed and optimized the protocols to enrich for sperm tips and I collaborated with the EMBL Proteomics Core Facility during mass spectrometry data acquisition and analysis. I calculated the cryo-electron tomograms from the different species and performed sub-tomogram averaging of TAILS in bovine samples. I contributed to the biochemical characterization of one TAILS candidate protein and its interaction with microtubules *in vitro*. I am contributing to the writing of the manuscript and the production of figures.

Abbreviations

Here follow the abbreviations included in this thesis, listed in alphabetical order.

BLI	**B**io-**l**ayer **i**nterferometry
Cryo-EM	**Cryo**genic **e**lectron **m**icroscopy
Cryo-ET	**Cryo**genic **e**lectron **t**omography
CP	**C**entral **p**air
DCDC2C	**D**ouble**c**ortin **d**omain-**c**ontaining protein **2C**
DCX	**D**ouble**c**ortin protein
dMT(s)	**D**oublet **m**icro**t**ubule(s)
EB	**E**nd-**b**inding protein
EM	**E**lectron **m**icroscopy
FACS	**F**luorescence-**a**ctivated **c**ell **s**orting
γ-TuRC	**Gamma-tu**bulin **r**ing **c**omplex
GDP	**G**uanosine **di****p**hosphate
GTP	**G**uanosine **t**ri**p**hosphate
IFT	**I**ntra-**f**lagellar **t**ransport
MT(s)	**M**icro**t**ubule(s)
MTOC(s)	**M**icro**t**ubule-**o**rganizing **c**entre(s)
ODF	**O**uter **d**ense **f**ibres
PBS	**P**hosphate-**b**uffered **s**aline
PCD	**P**rimary **c**iliary **d**yskinesia
PF(s)	**P**roto**f**ilament(s)
SEM	**S**canning **e**lectron **m**icroscopy
sMT(s)	**S**inglet **m**icro**t**ubule(s)
TAILS	**T**ail **A**xoneme **I**ntra-**Luminal** **S**piral
TEM	**T**ransmission **e**lectron **m**icroscopy
TIRF	**T**otal **I**nternal **R**eflection **F**luorescence

Acknowledgments

These past few years have been such an incredible journey which has taught me so much more than just science! I was lucky to share this experience with many people who have made my PhD time one of the best of my life.

First of all, **Johanna**, I still cannot believe you picked me as your first PhD student! I remember asking you via email if you really did offer me the position or if it was all a misunderstanding, even though you had shaken my hand and said, "Welcome to the team!". In some way, that feeling of incredulity still exists today, so thank you for always believing in me. You are the best supervisor I could have asked for and you have always encouraged me to try my hardest and give it my best, while making me feel reassured that it is ok to fall short at times. Your passion and your will to fight for what is right are truly inspiring and you are a role model whom I will always look up to in life.

Per W, thank you for always being supportive and for your helpful scientific input. You are an encyclopedia of knowledge and I feel like I learned something new every time we met. **Richard**, thank you for taking your time to check up on me and to make sure I was happy in my work environment since the very beginning. **Per S**, thank you for being the most efficient examiner ever!

Having spent over a year of my PhD being the only group member, I cannot express how happy I am to finally have so many amazing lab mates now! **Jake**, the results in this thesis would not be this cool if it weren't for you! I have always admired your work ethics and we have been such a great team together. Thank you for the fun times during our tips to Umeå and even though I didn't end up getting the climbing bug from you, I hope I made you proud with my few poor attempts! **Katharina**, you are the most confident and fiercest engineer I have ever met! Thank you for pushing me outside of my comfort zone and for creating a caring and safe space in the lab. But most importantly, thank you for all the cake, especially the one with splitting microtubules on it! You rock! **Dimitra**, our adopted group member and my favourite hairdresser! It's so cool that we first met at the beginning

of our master's (over six years ago!) and then ended up sharing office as PhD students. Thank you for always making me smile with your contagious (and loud :P) laughter, malaka! **Lisa**, you are the kindest soul I have ever met. You are always so genuine and a pleasure to be around! Whenever we need help in the lab, you are the one we often turn to and you are always ready to assist without complaint, so thank you for that. The precision and meticulousness of your lab work is something that I will strive for in my own career. And **Vaj**, thank you for joining our lab and taking over the flagella project. You have been such a welcome addition to the group and I have no doubt that you will be a brilliant student in the next years. I hope we will get the chance to hang out properly once the situation returns to normal!

A big thank you to **Lars**, **Bruno**, **Valida** and **Peter** for making our work at Lundberg possible. Thank you to the entire administrative staff, especially **Catarina**, for assisting us PhD students through all the messy paperwork. You have been a blessing! **Jeanette**, thank you for managing my teaching time. And thank you, **Ingrid** and **Johanna**, for bringing order to the chaos that are the course labs!

Thank you to all the collaborators that I've worked with. **Vašek**, you are so passionate and hard-working and your contribution to the project is extremely valuable. Best of luck with your PhD! Thank you to the Umeå team, in particular **Linda**, for teaching me the best negative staining protocol ever, and **Camilla** and **Michael**, for your ever-lasting patience with our broken grids and challenging data acquisitions. Thank you to the entire Rad lab in Boston: **Radhika**, **Nandini**, **Shuo**, **Christian**, **Qiong**, **Peii**, **Sitara** and **Farah**. You have all been so welcoming and you have made my time in your lab truly special. Thank you to the proteomics team at EMBL (especially **Mandy**, **Frank** and **Mikhail**) for dedicating so much time to my project. You have always made me enjoy my visits to EMBL, along with the delicious canteen food. Thank you to **John** and the rest of the Boulder team for helping out with tomography data analysis. **Anders** and **Magnus**, thank you for lending me your bioinformatics knowledge! **Anna**, **Soodi** and **Stefania**, it has been fun working with all of you and introducing you to the world of cryo-electron tomography. Best of luck with your projects! **Aleks** and **Rossella**, it was unfortunate that we didn't end up

working together for as long as we thought, but I am so thankful for how you took me under your wings at the very beginning of my PhD.

To **Björn** and his entire group (**Emelie**, **Darius**, **Yosh**, **Lisa**, **Laura**, **Ashish**, **Damasus**, **Ylber**, **Jens** and **Irena**) thank you for making the first floor such a lively place and for the nice company during lunch! To the entire second floor gang: **Tinna**, **Jessica**, **Viktor**, **Maja**, **Per**, **Greger**, **Adams**, **Swagatha**, **Lucija**, **Analia**, **Daniel**, **Giorgia**, **Andrea**, **Amke**, **Laras**, **Lidja**, **Weixiao**, **Matthijs**, **Ann**, **Manoop**, **Andreas**, **Owens**, **Doris** and **Jonathan** (including past members **Majo**, **Elin**, **Leo**, **Florian** and **Rajiv**), thank you for making the lab such a friendly space. You guys throw the most impressive parties!

To my fellow nerds on the fourth floor, thank you for so many fun times with boardgames and quizzes! I know that I have made some friends for life. **Martin**, we have been lab buddies since our master's thesis and even working in different labs afterwards has not changed that. Thank you for sticking by my side this entire time and for being a great friend! **Joana**, my favourite (ex-)neighbour and fellow South-European! Thank you for all the laughs and memes and I can't wait to get together again to play some Harry Potter trivia! **Stefanie**, I can't tell you how much I appreciate your interest in getting to know people, even though some of us were less cooperative than others at first! :P **Hanna**, you're crazy. And a bit weird. But we all love you for that. **Michelle**, you always have such a positive attitude and your enthusiasm at my quizzes is what inspires me to make more. **Emma**, I still feel sorry for ejecting you in Among Us when you were not the impostor! I promise I owe you one next time we play something :D **Sansan**, thank you for always providing a good chat and hot gossip! **Karl**, I am amazed at how many gross topics of discussion you manage to find during lunch! But you're forgiven because of your cool Christmas cards. **Simon**, thank you for fishing up some tunicates for me! It has definitely been one of the most memorable experiences of my PhD. **Alfred**, although I taught you lots of microbiology, I have a feeling that what you will really remember the most in the end is Italian swear words. **Carolina**, you went from being my teacher to becoming my teaching companion. You are such a passionate person with some true Colombian flare!

Anne, you have been like a mentor to me since my time in your lab and I am so glad that I got to keep working with you by teaching in your courses. I admire your positive, light-hearted attitude towards life and the passion that you put into your work. You are awesome!

To my old friends from our master's, **Rebecca**, **Anna** and **Karoline**, thank you for keeping in touch and organizing small reunions every once in a while. It's always fun to meet up! **Cristiana**, you are the first person I remember speaking to at the beginning of your courses and we have been close since then. I am so happy that we are still friends today and you and **Magnus** deserve lots of good books and good food. Hugs!

Mattia and **Monica**, my Venetian companions stranded in Sweden with me. Thank you for reminding me of home. **Fede**, you and **Luca** are the sweetest people I know and I am so grateful for your friendship. I am incredibly proud of you and I can't wait to meet up in person again.

To my **parents** and **sisters**, I know that it is tough for you too to be far away, but you have never let that stop you from encouraging me all the way. Thank you for always pushing me to chase my dreams, wherever in the world they might take me. I am proud of the person that I have become and it is all thanks to you.

To my **aunt** and my **cousins**, thank you for always making me feel like a superstar! Un rigraziamento ai miei **nonni**, che mi supportano sempre anche da lontano.

Till hela **familjen Landers** samt **Monica** och **Bert**, tack för att ni blev min svenska familj. Ni har alltid fått mig att känna mig som hemma.

Rasmus, you are the one who made this all possible. Who knew that playing online games on Minecraft would change my life? After living together in a one-room apartment for six years, I don't see how anything could break us! I am so incredibly proud of how far we have both come, by learning about each other and ourselves. Thank you for accepting all sides of me. I love you and I am excited to see how many cool adventures our life together will bring us.

Table of contents

Chapter 1

Introduction

1.0 Aim of the thesis

This thesis compiles three research papers which investigate the ultrastructure of the human flagellar tip, aiming to reveal its specific composition and functions. In these studies, the sperm flagellum was selected as a model system and cryo-electron microscopy and cryo-electron tomography were adopted as the main techniques of choice.

In this first chapter, the basic concepts regarding microtubule biochemistry and flagellar ultrastructure and function are illustrated.

Chapter 2 gives a general introduction to the different electron microscopy techniques employed in the papers presented.

The remaining chapters present and discuss the results published in the attached papers:

Chapter 3 summarizes the findings reported in **Paper I**, which offers an ultrastructural description of the anatomy of the human sperm tip. The results revealed high intercellular structural variability and new microtubule architectures.

Chapter 4 focuses on **Paper II**, which describes the discovery of TAILS, an extensive inner microtubule structure that specifically localizes to the distal tip of the sperm flagellum. Different hypotheses on TAILS's function are discussed.

Chapter 5 illustrates and discusses the multi-pronged approach we designed to identify the TAILS complex and its function, as it is presented in **Paper III,** which is an unpublished manuscript. This work includes a higher-resolution of the TAILS structure, the first ever flagellar tip proteome and a cryo-electron tomography investigation of the conservation of TAILS among different species.

1.1 Microtubules

Microtubules (MTs) are eukaryotic components of the cytoskeleton which perform a multitude of cellular functions. They are hollow and flexible tubes made of tubulin and are intrinsically dynamic, which makes them an extremely versatile cellular structure. They were originally discovered in the early 60's in electron micrographs of actively dividing cells [1, 2], where they formed the mitotic spindle. The term "microtubule" was coined soon thereafter when cytoplasmic MTs were observed in plant [3] and hydra [4] sections.

1.1.1 Tubulin

MTs are polymers of tubulin heterodimers (Figure 1.1). Each heterodimer consists of one α-tubulin and one β-tubulin molecule and measures approximately 8 nm in length, 4 nm per tubulin [5, 6]. The two monomers are ~50 kDa globular proteins with 40% sequence identity and nearly identical structure, with the main difference being an 8-residue loop insertion in α-tubulin compared to β [5]. Both proteins exist in a variety of isoforms and can undergo additional post-translational modifications, which together define the "tubulin code" [7, 8]. Each tubulin monomer binds to a GTP molecule, however only the nucleotide bound to the β subunit is hydrolysed during polymerisation [9], which is the mechanism underlying the dynamic behaviour of MTs [10–13].

1.1.2 Microtubule structure

In MTs, the tubulin heterodimers interact longitudinally with each other, making head-to-tail contacts between the adjacent α and β subunits, forming protofilaments (PFs). Multiple PFs are in lateral contact with each other, forming the distinctive hollow tubular structure that is a MT [14, 15]. Since the structural unit of a MT is a heterodimer, each end of an individual MT is crowned by a different tubulin subunit, making them polar filaments. The end terminating with α-tubulin is defined as the minus-end, while the one with β-tubulin is called the plus-end.

The number of protofilaments in a MT is variable, depending on the polymerization environment. *In vitro*, if tubulin reaches a threshold critical concentration, polymerization occurs spontaneously [16, 17], generating populations of MTs with a number of PFs typically ranging between 11 and 16 [15, 18–21]. *In vivo*, the PF number is strictly regulated by the cell, but the preferred number varies between different organisms [22]. The nematode *Caenorhabditis elegans* for example has MTs with 11 PFs [23, 24], while in most model organisms, including humans, MTs usually have 13 PFs and a 25-nm diameter [22, 25, 26]. This is due to the major cellular MT nucleating factor, γ-TuRC (gamma-tubulin ring complex), which imposes a 13-PF symmetry and is widely conserved among eukaryotes [27–29].

While heterodimers within the same PF always associate head-to-tail with contacts between heterologous α-β subunits only, lateral

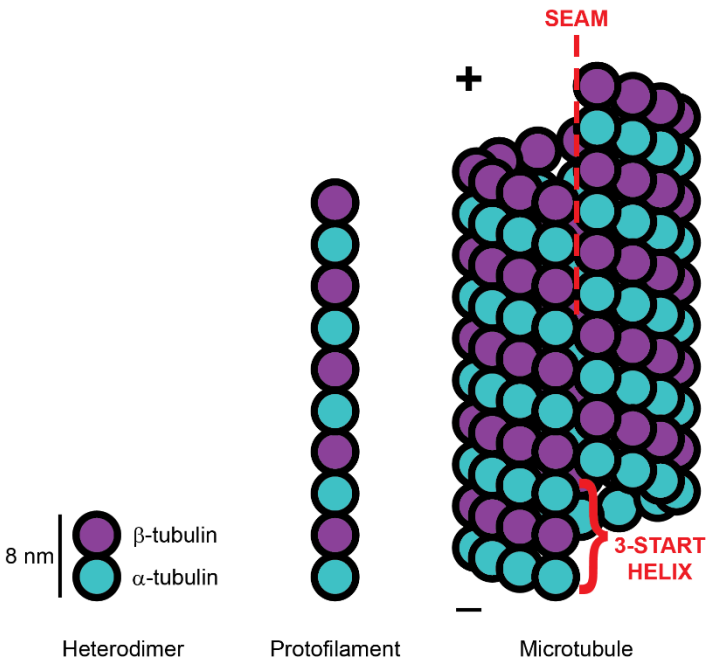

Figure 1.1: Microtubules are polymers of tubulin. Free tubulin exists in heterodimers of α and β-tubulin. Heterodimers interact longitudinally head-to-tail to form PFs, which interact laterally to form MTs. MTs in most model organisms have 13 PFs and a B-lattice except at the location of the seam, which has an A-lattice.

contacts between protofilaments can involve interactions between heterologous (α-β) and homologous (α-α or β-β) subunits. The lateral association between PFs determine the MT lattice, which is either called the A-lattice or the B-lattice for heterologous or homologous lateral interactions, respectively. Both *in vitro* and *in vivo* MTs commonly include a mixture of the two lattices, with the B-lattice being more predominant [30–32]. The typical 13-PF MT has a B-lattice along its entire wall except for between two PFs, where lateral contacts between heterologous subunits form an A-lattice. This structural feature is called the MT seam [33]. Starting from the seam, following the lateral contacts between subunits around the 13 PFs of the MT wall results in a shift of 12 nm along the MT longitudinal axis, equivalent to the length of 3 monomers along one PF. Such a MT is therefore said to have a 3-start helix. MTs can have variable helix-start numbers as well as a variable amount of seams [34], a feature that has been observed even along one same MT [19].

1.1.3 Dynamic instability of microtubules

MTs are dynamic structures that spontaneously undergo phases of growth and shrinkage, even *in vitro* [10, 11]. This innate property of MTs is referred to as dynamic instability and it can be described as a cycle of four events: growth, catastrophe, shrinkage and rescue [35] (Figure 1.2). When tubulin is present in a GTP-rich environment and at concentrations higher than its critical threshold, spontaneous MT nucleation occurs [36]. Soluble GTP-tubulin then associates in a bent conformation on growing PFs [37] at either end of the newly nucleated MT seed, leading to polymerization, which is distinctive of the growth phase. Although MTs elongate on both ends, polymerization occurs faster at the plus-end [38]. MTs are therefore not only structurally polar, but also functionally. As new GTP-tubulin heterodimers are added onto the MT, their GTP molecule is induced to hydrolyse into GDP [9]. This causes a conformational change in α-tubulin which leads to an overall lattice compaction, inducing strain in the MT structure [13, 39]. Polymerization proceeds during the growth phase as long as the

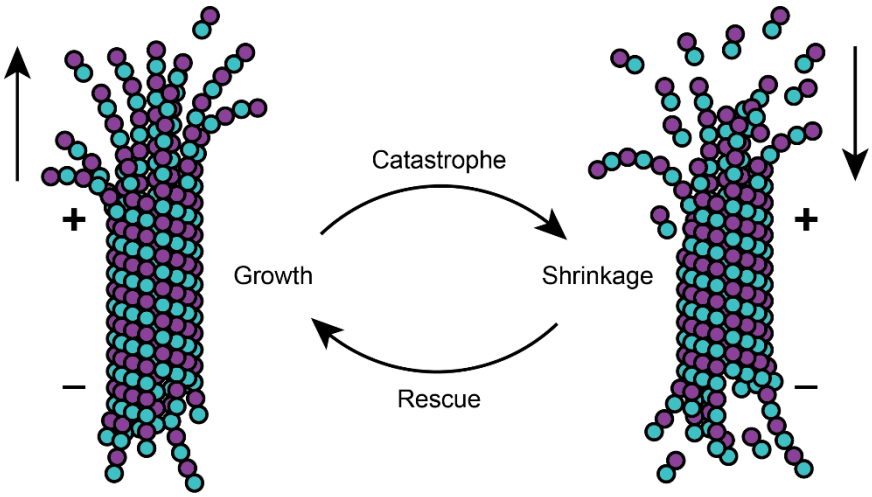

Figure 1.2: The dynamic instability of microtubules. MTs have the intrinsic ability to go through cycles of polymerization and depolymerization *in vitro*. The process involves four phases that follow one another in a cycle: growth, catastrophe, shrinkage and rescue.

association rates of new GTP-tubulin heterodimers are higher than the GTP hydrolysis rates. The association of GTP-tubulin ensures a stable GTP cap at the growing end, which stabilizes the entire MT, although tubulin dimers along the rest of the MT are in a GDP state [10]. As free tubulin associates at the MT ends and its concentration lowers, MT growth stalls and the GTP hydrolysis rates prevail on the association rates. The GTP cap is lost and the strain on the lattice is released by the bending of the longitudinal contacts between heterodimers, which triggers a catastrophe event [10, 40, 41]. The lateral contacts between dimers are weakened and the PFs start separating, leading to rapid MT depolymerization and to the shrinkage phase [39]. As the concentration of free tubulin rises again, the shrinkage eventually halts due to the association of new GTP-tubulin, which is known as the rescue [41]. After a rescue event, a new GTP-cap is formed, polymerization resumes and MTs re-enter their dynamic cycle with a new growth phase.

1.1.4 Cellular functions of microtubules

Due to their dynamicity, MTs are versatile structures that the cell employs to perform multiple functions in different processes. Cytoplasmic MTs are ubiquitously present in eukaryotes where they

provide a physical support for organelle positioning and cargo trafficking around the entire cell. They function like cellular highways, where molecular motors can bind and move along, transporting various cargos with them [42]. A notable example of MT-based transport is found in neuronal axons, which can span lengths in the order of meters. For such distances, diffusion is an inefficient method of molecular transport, therefore MTs extend throughout the entire axon, enabling the trafficking of cellular components, such as nuclear products and synaptic vesicles [43, 44].

During cell division, MTs serve another specialized function, as they are organized into the mitotic spindle [1, 2]. The spindle binds to the kinetochore of sister chromatids and is directly responsible for chromosome segregation during anaphase [45–47].

The cytoskeleton and MTs in particular are involved in cell migration as well, as it was observed that locomotion is inhibited in the presence of drugs interfering with MT stability [48, 49]. Their role is to establish movement directionality [50] and maintain cell integrity during migration [51].

Lastly, MTs form the cytoskeleton of eukaryotic flagella, where they provide structural support (as in non-motile flagella) and generate active movement in combination with motor proteins (as in motile flagella) [52]. Flagellar MTs and their associated proteins are the focus of this thesis and they are discussed in detail in the next section of this chapter.

1.1.5 Microtubule associated proteins

It is the intrinsic dynamic instability of MTs that makes them such a versatile tool for the cell. However, their activity needs to be regulated very precisely to perform their wide variety of functions. This tight regulation is mediated by hundreds of MT associated proteins (MAPs), which control every MT-related process [53].

In vivo, MT-organizing centres (MTOC) like the centrosome are responsible for MT nucleation by recruiting γ-TuRC complexes [54, 55]. The γ-TuRC acts as a template for polymerization of 13-PF

MTs by recruiting soluble tubulin α-β heterodimers and facilitating their lateral interactions [29, 56, 57]. γ-TuRC can also cap the MT minus-end [58] and be recognized by anchoring proteins which determine the MT cellular localization [59, 60].

MT growth is actively promoted in the cell by proteins containing an array of TOG-domains, either by facilitating polymerization or by suppressing catastrophe events [61]. Proteins containing TOG-domains recruit free tubulin dimers, bring them to the MT growing end and facilitate their incorporation into PFs [62].

The growing plus-end of a MT can be tracked by members of the doublecortin family, like DCX, which can nucleate 13-PF MTs *in vitro* just like the γ-TuRC [21, 63]. DCX has two MT-binding domains which act sequentially to stabilize MTs [64], first by recognizing the curved MT lattice at the growing tip [65] and then by binding to the straight lattice of the polymerized MT to prevent catastrophe [64].

The end-binding (EB) protein family also includes MAPs which bind to the MT plus-end, both *in vitro* [66, 67] and *in vivo* [68–70]. Rather than tracking PF curvature like DCX, EB1 recognizes the nucleotide state of tubulin and it preferentially interacts with the GTP cap [71]. EB1 favours lateral interactions between PFs, creating and inducing the closure of tubulin sheets *in vitro* to form 13-PF MTs [66].

Kinesins and dyneins are motor proteins that translocate on PFs and can transport cargo towards the MT plus-end or minus-end respectively [42, 72]. In motile flagella, it is dynein arms anchored to one MT and moving along the adjacent one that cause the flagellar beat [73, 74].

1.1.6 Microtubule inner proteins

While much is known about MAPs interacting with the MT outer surface, an increasing amount of evidence is showing that many MT regulatory processes take place in their lumen as well. MAPs that perform their function in the MT luminal space are referred to as

MT inner proteins (MIPs) [73]. Luminal densities in cytoplasmic MTs have been observed for decades [75–78], although their identification still remains a challenge. The first protein to be reported to have an affinity for the MT luminal wall was a member of the neuronal Tau protein family [79]. Since then, more observations of MIPs have been reported, ranging from small and globular, like MAP6 [80], to long and extensive, like the actin filaments found in the MT lumen of cell projections [81]. The identification and subsequent biochemical characterization of MIPs has become more feasible only in recent times, thanks to advancements in electron microscopy [82]. Flagellar MTs are particularly suitable for such investigations and multiple flagellar MIPs have been identified in protists [83–88]. They have been shown to be crucial in maintaining proper flagellar structure and function [85, 86].

As presented in **Paper II**, our investigation of human sperm tip MTs revealed a novel extensive luminal structure which we named TAILS. This thesis presents our work in characterizing this new structure biochemically and functionally.

1.2 Eukaryotic flagella

Eukaryotic flagella, also called cilia (the two terms will be considered synonyms in this thesis), are membrane-bound organelles protruding from the cell surface and supported by a MT cytoskeleton [89]. They can be found in unicellular organisms, as in the commonly researched models *Chlamydomonas reinhardtii*, *Trypanosoma brucei* and *Tetrahymena thermophila*, as well as in multicellular organisms. In humans, almost every non-dividing cell has one or more flagella. They can be motile or non-motile and they perform functions ranging from cell movement to signal transduction [52].

1.2.1 Flagellar ultrastructure

The overall ultrastructure of flagella is widely conserved among eukaryotes [89], which is why protists are commonly used as model

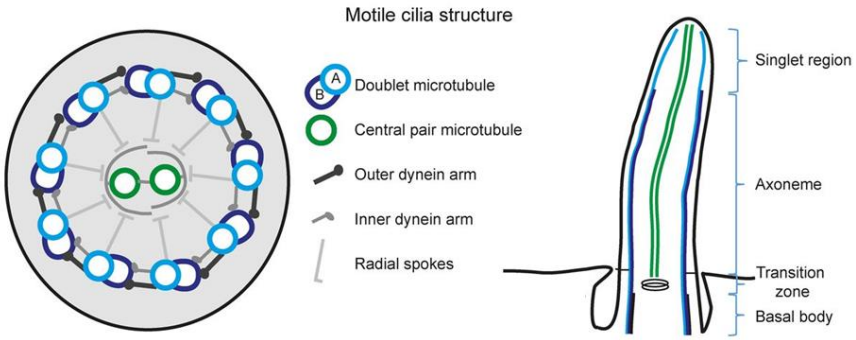

Figure 1.3: The ultrastructure of motile flagella/cilia. The MT cytoskeleton has a symmetrical 9+2 arrangement called the axoneme. At the flagellum tip, only sMTs are found. Reproduced from [104] (https://creativecommons.org/licenses/by-nc-nd/4.0/).

organisms [90]. The flagellum is attached to the cell via the basal body, which is composed of an array of 9 MT triplets that nucleate the flagellar MTs [91, 92]. Each triplet MT includes an A-tubule, which is complete with 13 PFs, and a B- and a C-tubule which are only composed of 10 PFs each and are attached to the previous tubule of the triplet. The MTs extend into the flagellum as doublet MTs (dMTs), which include a complete A-tubule and an incomplete B-tubule. At the termination point of triplets the flagellar transition zone is found, a region with complex structural elements such as the basal plate [89, 92–94]. The transition zone has been proposed to act as a selective barrier between the cytoplasm in the cell body and the flagellar cytoplasm [94]. Throughout most of its length, the flagellum presents a highly conserved symmetrical arrangement of MTs and associated proteins, which is called the axoneme. In non-motile flagella, the axoneme is usually composed of a circular arrangement of 9 dMTs (9+0 type), which is often broken by one or two dMTs shifting to the middle of the axoneme, referred to as a 9-variable axoneme (9v type) [95–97]. In most motile flagella, two additional individual MTs are found in the middle of the 9 axonemal dMTs (9+2 type), elongating from the basal plate in the transition zone. Together with auxiliary structures, these MTs form the central pair (CP) complex, which is connected to the dMTs through 9 radial spokes [98] and is thought to modulate the flagellar beat [99, 100]. The CP itself however is not required for movement, since the

flagellar beat is generated by dynein motors running on dMTs while being anchored to the adjacent doublet, causing torsion in the axoneme [26, 73, 74, 101]. In addition, cases of motile flagella lacking CP have been reported [102, 103]. At the distal tip of the flagellum, dMTs progressively terminate as the flagellar membrane tapers. Both in motile and non-motile flagella, the dMTs transition into singlet MTs (sMTs) [26, 97, 104–106], however the MT transition and termination patterns vary greatly between organisms and cell types [107]. The large morphological and ultrastructural variability observed at flagellar tips is what inspired the work presented in this thesis. More details regarding the ultrastructure of tips in motile flagella are discussed further later in this chapter.

Based on their specific function, some flagella evolved specialized structures, which can dramatically differ from the typical flagellar structure described so far. Examples of specialized flagella are the human olfactory cilia [108], neuronal sensory cilia in *C. elegans* [109] and the rod cell cilia in the retina [110].

1.2.2 Flagellar function and ciliopathies

Flagella can perform different functions depending on the organisms or cell type they belong to. Motile flagella are used in unicellular organisms, as well as in the spermatozoa of many species, for cell locomotion [73, 111–114]. Motile flagella can also be found in tissues in multicellular organisms, as in the tracheal epithelium or in the brain ventricular cavities, where their function is to induce a flow of mucus or fluid, rather than cell movement [115–117]. Flagellar propulsion of fluid is important in the early stages of mammalian development, where motile flagella generate a leftward flow in the extraembryonic fluid at the node during gastrulation to determine the left-right symmetry of the body [103]. Additionally, both motile and non-motile flagella have been reported to possess sensorial functions, acting as antenna-like organelles that the cells use to investigate their surroundings [118–121], or as signalling hubs for various pathways [122, 123].

The flagellum is a complicated biological machine consisting of hundreds of different components [124–127], which need to properly work together in a tightly coordinated fashion. If any of these components fail to perform their function, the entire flagellar activity can be compromised. For this reason, a plethora of genetic defects that affect flagella exist in humans [128–132] and they cause pathologies which are collectively referred to as ciliopathies [133] or primary ciliary dyskinesia (PCD) for motile flagella specifically [134–136]. The conditions caused by PCD vary in nature and severity between patients, but they often include chronic respiratory infections, cognitive impairment, infertility and situs inversus [135]. To better understand the molecular mechanisms underlying these pathologies, it is critical to elucidate how functional flagella work. The studies included in this thesis aim to fill the knowledge gap regarding the ultrastructure of human flagellar tips, which have been strangely overlooked compared to other flagellar features and species.

1.2.3 Flagellar distal tip

The flagellar distal tip is of particular interest to us as it hosts important processes for flagellar and cellular homeostasis. One example is the components of the Hedgehog pathway, which is important in embryonic development and in tissue homeostasis [123]. The MT plus-end is also found at the flagellar tip [68, 137], which is important for MT growth during ciliogenesis [138] and regulation of their dynamic instability [139]. Various cargo is also carried along the axoneme in both directions by the intra-flagellar transport (IFT) system [140]. Consequently, the flagellar tip is a trafficking hub where cargo needs to be loaded or unloaded and the transport machinery needs to be assembled or disassembled [141].

Despite its important functions, the human flagellar tip has remained relatively unexplored. We recently reviewed the literature regarding the flagellar tip in multiple organisms and cell types, revealing a remarkable variability in ultrastructure [107]. Therefore, its architecture seems to be far from widely conserved among

eukaryotes, as is normally observed for the axoneme. Based on these observations, we wondered how the structure of human flagellar tips compares to the ones in model organisms. We therefore set out to fill this knowledge gap by studying the ultrastructure of human sperm flagella. Our techniques of choice were based on electron microscopy and our main findings are compiled in this thesis as part of **Papers I-II-III**.

Chapter 2

Electron microscopy

Electron microscopy (EM) is arguably the imaging technique which is best suited for investigation of sub-cellular structures on a molecular level. For this reason, it became our investigation method of choice. As we were studying the structure of the sperm flagellum, different EM techniques were applied to the project. This chapter offers a general overview of these methods, with a focus on EM of biological samples.

2.1 Basics

In microscopy, the final image resolution is limited by the wavelength (λ) of the radiation used for imaging (in an ideal system $r = \lambda/2$). In optical microscopy, the samples are visualized via visible light (λ ranging 400-700 nm), which allows to reach a maximum resolution of approximately 200 nm. While this make optical microscopy more than sufficient to observe tissues, entire cells and even organelles, it is not enough to reveal the molecular details of cellular structures. Instead, electron microscopes can reach remarkably higher resolutions by using electrons over visible light as their illuminating radiation. Electrons have a much smaller wavelength and can theoretically provide an image resolution of under 2 pm (= 0.02 Å), which is below the size range of individual atoms.

The way that electrons are used to produce an image is conceptually similar to how light is producing an image in optical microscopy. In both cases what is needed is a radiation source, lenses to focus the radiation, a sample and a detector. Light bulbs generate photons which are focused with optical lenses onto the glass slide with the sample and the image can be visualized by the user directly or with a camera. Similarly, in an electron microscope a current is run through an electron source, which can be as simple as a tungsten

filament or more advanced like a LaB_6 crystal filament or a field emission gun, which has the most coherent electron beam. The generated electron beam is focused with magnetic lenses onto the sample, which is supported by a meshed metal disc called an EM grid (Figure 2.1). The electrons are then recorded with specialized cameras, like the direct electron detectors found in high-end microscopes for biological imaging.

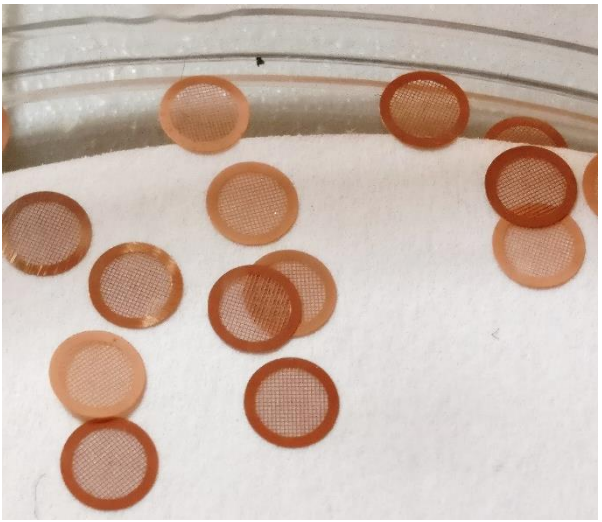

Figure 2.1: Electron microscopy grids. The image shows copper EM grids of about 5 mm in diameter. The mesh of the grid is visible.

When electrons hit a sample, they are either scattered away in different directions or they penetrate and pass through the sample. In both cases, the electrons will carry with them information from their interaction with the sample, which can be recorded. When the scattered electrons are used for recording an image, the technique is referred to as scanning electron microscopy (SEM), which provides images of the three-dimensional surface of the sample. When the penetrating electrons are recorded instead, the technique is called transmission electron microscopy (TEM), which generates images representing a two-dimensional projection of the entire three-dimensional structure of the sample, including its inner features. In this thesis, only TEM work was performed, since our scientific question regarded the nature of structures inside the cell.

While the theoretical resolution of electron microscopes reaches the atomic scale, for biological samples this is in practice extremely complicated and it was only achieved for the first time a few months ago [142, 143]. The main limitation comes from the fact that atomic details in biological samples are easily damaged during the imaging itself or during sample preparation [144]. Electrons carry comparable or higher energy than X-rays (λ = 0.01 to 10 nm), which causes radiation damage on the sample during exposure, limiting the resolution [145]. In addition, most sample preparation methods introduce artefacts by damaging the biological material on a molecular level [146]. The main need for sample preparation protocols comes from the fact that the imaging occurs in a vacuum. Electrons inside the microscope travel in a vacuum, as gas molecules would scatter the electrons away, making it impossible to focus them into a beam. Consequently, biological samples cannot be directly inserted into the microscope, as they contain water that would evaporate, and instead need to be suitably prepared [147]. There are multiple sample preparation protocols which tackle this problem in different ways, depending on the nature of the sample and the scientific question behind the experiment [147, 148]. In most used techniques, the sample is dehydrated and coated with heavy metals or alternatively quickly frozen to liquid nitrogen temperatures. The rest of this chapter briefly introduces the sample preparation and imaging techniques employed in the work presented in this thesis.

2.2 Room temperature electron microscopy

When samples are imaged at room temperature, they need to be in a dehydrated state to avoid water evaporation, which would compromise the vacuum and damage the sample's ultrastructure. In addition, heavy metals are used to stain the sample to increase the contrast in the images. Common heavy metal salts used in EM are uranyl acetate, osmium tetroxide and lead citrate [148]. These elements have a high electron density, which causes a strong scattering of the incoming electron beam. For this reason, the image

appears dark in areas where the heavy metals have deposited, providing good contrast between the sample's features and the background. Therefore, the obtained images do not show the biological material directly, but rather the deposition of heavy metals on and around it which will always limit the resolution one can achieve with this sample preparation [144].

2.2.1 Negative staining

The negative staining protocol provides a quick and easy way of preparing a sample for EM [149–151], although it only highlights the outline and the features on the surface of the sample (Figure 2.2). The sample is applied as a liquid solution or suspension to a glow discharged EM grid, which means it has been exposed to charged plasma to render its surface hydrophilic. Most of the sample volume is blotted away with filter paper and the grid is washed twice in water before staining it in a heavy metal salt solution (which in the work presented here was uranyl acetate, 2% in water). After a final

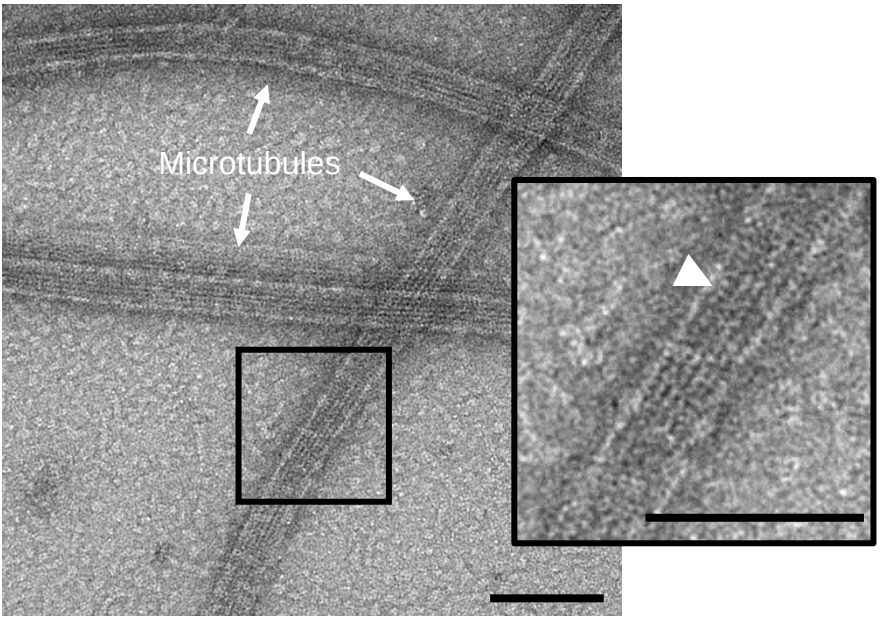

Figure 2.2: Electron micrograph of negatively stained microtubules. The stain deposition creates contrast around the sample, highlighting the outline of the microtubules and their surface features. Protofilaments and individual tubulin monomers are visible as well (white arrowhead). Scale bars are 100 nm.

blot, the grid is let air dry for at least a few minutes before imaging. As the stain solution dries out, the heavy metal salts deposit around the sample, forming an electron-dense crust which highlights the sample's outline. The biological material therefore appears more electron translucent compared to its outline, which is why this technique is called negative staining [150].

The advantage of negative staining is that it can be applied to any sample in solution or suspension, from individual proteins to membrane vesicles and even cells [152]. The preparation is quick and easy to perform and the samples are ready for imaging shortly after staining [149, 152]. On the other hand, only the shape, concentration and distribution of the sample can be visualized with this method. No information regarding intracellular structures can be gained and high-resolution structural details are hidden, as the features visible in the image are limited to the deposition of stain. This technique is often used to assess sample quality before advancing to more complicated preparation protocols, such as plunge-freezing which is described later in this chapter.

2.2.2 Cryo-fixation and plastic embedding

The thickness of a sample determines its transparency to electrons. Samples thicker than 400-500 nm are harder to image because they scatter electrons strongly and the resulting image looks dark. For this reason, when there is an interest in visualizing the internal structure of a large object like a cell or organism, the sample needs to be sectioned. The sample must be fixed prior to sectioning and this can be done chemically or physically. Chemical fixation involves cross-linking of macromolecules in a non-specific manner, which is preferably avoided since it introduces major artefacts and deformations in the sample's structure [138, 153, 154]. An alternative is cryo-fixation in the form of high-pressure freezing, where the sample is cooled down to -180°C in ~25 ms with liquid nitrogen [153, 155]. The freezing process takes place under high pressure (~2100 Bar), which prevents ice crystallization and preserves the native biological ultrastructure of the sample. If ice

crystals formed in the sample, they would expand in volume and therefore push around the biological material, compromising the structural integrity of the cell [156]. After cryo-fixation, the sample is dehydrated by slowly replacing its water content with acetone. Usually, a cocktail of fixatives and heavy metals are also introduced at this step to preserve the cellular structure and provide contrast [153, 156]. The acetone is then replaced with a plastic resin which is polymerized and once it has hardened, the sample is completely embedded in it and can be taken to room temperature to be sectioned with an ultramicrotome. Before visualization, the sections are stained with solutions of heavy metal salts like uranyl acetate and lead citrate [157]. The stain deposits differently on the various sub-cellular structures, creating contrast between them.

Cryo-fixation is a powerful method of physical fixation which grants great insight into the sub-cellular structures of entire cells and organisms (Figure 2.3). Just like in negative staining however, heavy metals are used for enhancing the contrast. Ultrastructural studies at atomic resolutions are therefore unfeasible after such preparation.

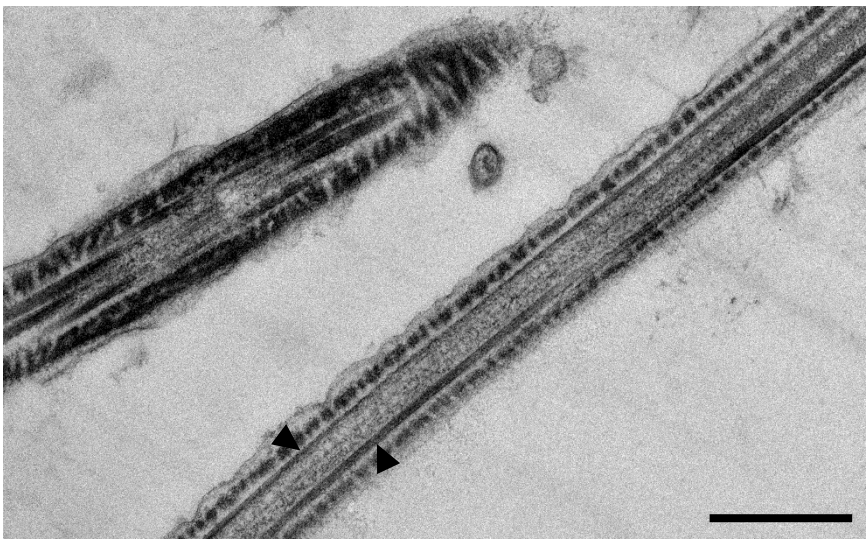

Figure 2.3: High-pressure frozen and plastic embedded bovine sperm cells. The thin (~80 nm) section shows a longitudinal view along the flagellum of a spermatozoon. Inner structures like axonemal MTs are visible (arrowheads). Scale bar is 500 nm.

2.3 Cryo-electron microscopy

An alternative to sample dehydration is imaging the specimen while frozen at liquid nitrogen temperatures, a procedure called cryo-electron microscopy (cryo-EM) [158]. This prevents water evaporation from the sample and offers the advantage of maintaining the biological structures in their native hydrated state. No heavy metals are added to the sample, whose biological density can be observed directly (Figure 2.4). Its high-resolution native structure is preserved but the compromise is poor contrast and signal-to-noise ratio. This can partially be compensated for by imaging at high defocus, which improves contrast at the expense of resolution, in cases where high-resolution details are not needed. Substantial technological improvements of the detectors and the microscopes themselves have helped to overcome these challenges in the past few years, resulting in the so-called “resolution revolution” [82], which allowed cryo-EM to become an established structural biology technique alongside X-ray crystallography. To underline how much cryo-EM has impacted cell and structural biology in the past decades, the Nobel Prize in Chemistry in 2017 was awarded “for developing cryo-EM for the high-resolution structure determination of biomolecules in solution" [159].

2.3.1 Plunge-freezing

Samples in aqueous solution or suspension can be prepared for cryo-EM by plunge-freezing. The concept behind the technique is quite straight-forward. One drop of sample (between 3 and 5 µm) is applied to a glow-discharged EM grid and most of its volume is blotted away with a filter paper. The blotting step is critical to create a very thin layer of aqueous sample on the grid. The thinness of the sample ensures a rapid freezing and more contrast during imaging, as thick samples give noisier images. Then, the sample is quickly plunged into a liquid cryogen at -180°C, causing its water molecules to freeze before they have time to arrange themselves into crystals.

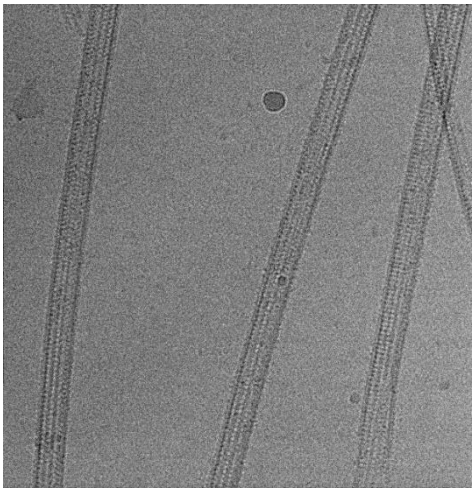

Figure 2.4: Cryo-electron micrograph of microtubules in vitreous ice. The biological density of the microtubules is directly visualized without staining.

The resulting ice forms in a vitreous state [160], which preserves the native biological structures as they were in the instant they froze [161].

The samples in the studies attached to this thesis were prepared with plunge-freezing machines like the Vitrobot (**Papers I**, **II** and **III**) and the Leica GP (**Paper III**). The blotting time ranged between 4 and 8 seconds and the cryogen used for freezing was ethane, which at -180°C ensures a more rapid freezing than nitrogen due to being further away from its boiling temperature [162, 163].

2.3.2 Cryo-electron tomography and sub-tomogram averaging

Since TEM produces two-dimensional projection images, information on the three-dimensional arrangement of the sample is lost in a single micrograph. This information can be recovered by acquiring and computationally combining multiple projection images of the same sample viewed from different tilt angles. This reconstruction technique is called electron tomography [164] and it can be performed at room temperature on thick sections of plastic-embedded material, as well as on plunge-frozen samples, which is then called cryo-electron tomography (cryo-ET). This powerful

technique provides insight into the native sub-cellular localization of structures on a molecular scale.

Just like any other scientific technique, this method comes with its own set of artefacts. During the acquisition of tilted images, it is physically impossible to image the sample from all directions since at higher tilts the EM grid bars cover the sample and the electrons need to penetrate increasingly thicker volumes of ice. Therefore, a common cryo-ET acquisition includes a range of tilts between -60° and 60°. Thus, information from some angles is missing in the final reconstruction, known as the missing wedge. This artefact causes the elongation of features that are perpendicular to the grid's rotation axis, resulting in anisotropic resolution in the tomogram [165]. Additionally, to avoid radiation damage, the illumination of the sample must be decreased dramatically for each individual image, as up to 60 images need to be acquired on the same area of biological interest. This causes poor contrast and high noise in the images, which complicates data analysis.

If a structure of interest is present in multiple identical copies in the cryo-ET dataset, it is possible to improve its signal-to-noise ratio and reveal its molecular details with an approach called sub-tomogram averaging. This is a computational extraction and iterative cross-correlation alignment of sub-volumes (also called particles) containing repeats of the structure of interest. By doing so, the structurally consistent features of the object become enhanced over the general noise, which is averaged away instead. Multiple software packages that perform sub-tomogram averaging are available as open-source material, such as PEET [73], Dynamo [166] and RELION [167].

Cryo-ET and sub-tomogram averaging have been crucial for the work presented in this thesis, as they allowed us to investigate the previously unknown molecular structure of sperm tips. In our studies, tomograms were calculated with the IMOD software package [168] and PEET was used to perform sub-tomogram averaging of TAILS in MTs [73].

2.3.3 Single particle analysis

While cryo-ET and sub-tomogram averaging are incredibly powerful techniques to study cellular structures in their native environment, they are limited by the noise present in the collected data. Noise lowers contrast, which often makes it difficult for the user to recognize the structure of interest in a crowded cellular environment and to select it for averaging. This is particularly true for smaller structures like protein complexes or even individual proteins. In this case, high-resolution structural studies can still be performed if the object of interest is purified from its environment. Two-dimensional images of identical copies of the same structure in aqueous environment can be combined to obtain molecular three-dimensional information. Instead of tilting the sample, the three-dimensional information is provided by each particle being imaged in a random spatial orientation as it was in solution before plunge-freezing. The processing protocol, commonly executed with the RELION package [169], is called single particle analysis [170] and it can yield much higher resolution structures of the sample compared to sub-tomogram averaging, now even reaching atomic resolution [142, 143]. One reason for this is that there is no need to dilute the amount of electron dose among multiple images like in tomography, yielding higher contrast and more information. Secondly, the biological density of the object of interest is imaged without it overlapping with other structures like in a crowded cellular environment, reducing noise. Of course, the drawback is that the structure of interest needs to be purified and isolated from its native environment, potentially altering its native state. However, the two approaches of sub-tomogram averaging and single particle analysis can be very informative when combined together, providing insight into the native cellular environment of an object of interest as well as its high-resolution structural details [171].

Single particle analysis was applied to our project to reveal the structure of TAILS in MTs on a molecular level, as discussed in Chapter 5. A combination of the RELION and *cis*TEM [172] software packages was used for this purpose.

Chapter 3

Ultrastructure of human sperm tips

After assessing the ultrastructural variability of motile flagellar tips in different organisms [107], our goal was to elucidate how those structures compared to the flagellum in humans. The spermatozoon presented itself as the ideal model for ultrastructural studies of the flagellum with cryo-ET, as it consists of only a small head and a long flagellum as a tail, which is thin enough for direct visualization. Additionally, ejaculate can be collected non-invasively from patients and it can be plunge-frozen for cryo-EM without the need for any prior preparation. A detailed cryo-ET investigation of the human sperm ultrastructure, with a focus on the flagellar distal tip, is presented in **Paper I**.

3.1 Anatomy of the mammalian spermatozoon

The spermatozoon is the animal male gamete, whose function is to fertilize the female gamete, the oocyte, achieving fecundation. It evolved into an extremely specialized cell with a peculiar anatomy. Unlike most eukaryotic cells, the spermatozoon only carries a minimal cytoplasmatic volume and it lacks many common cellular organelles, such as the endoplasmic reticulum, the Golgi apparatus and lysosomes. The mammalian spermatozoon has a small cell body, called the head, and a long motile flagellum, called the tail. The tail is divided into the middle piece, the principal piece and the end piece based on the presence or absence of auxiliary structural features [173–175] (Figure 3.1). The total length of the human sperm cell is approximately 60 µm, however variations in the order of hundreds of microns do occur between different mammalian species [176].

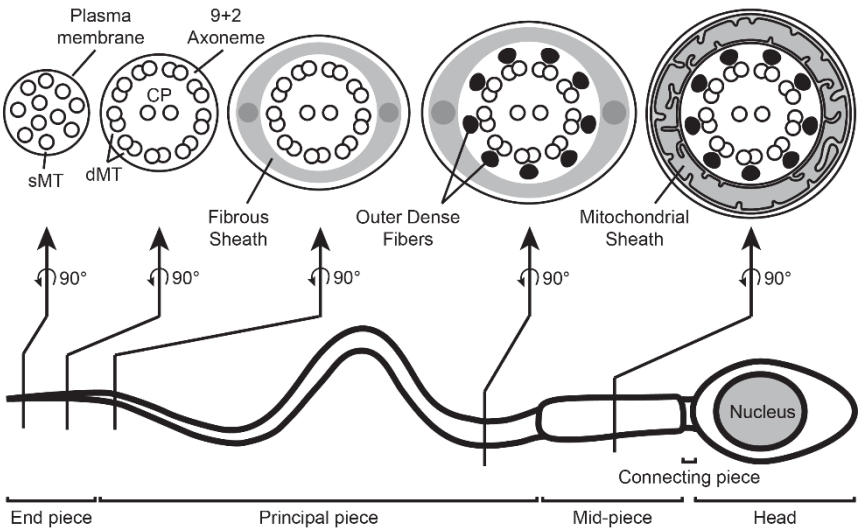

Figure 3.1: Anatomy of the mammalian spermatozoon. The mammalian spermatozoon consists of a small cell body called the head and a long flagellum called the tail. The tail is attached to the head through the connecting piece and it is structurally divided into the middle piece (or mid-piece), principal piece and the end piece, based on which auxiliary structures are present or absent. Figure reproduced with permission from **Paper I**. (https://creativecommons.org/licenses/by-nc-nd/4.0/)

3.1.1 Head

The head is the main cell body of the spermatozoon. It contains the nucleus which carries the haploid genome of the cell in a highly compacted and condensed state [177–179]. On its anterior side, the head contains the acrosome, a membranous organelle which carries the hydrolytic enzymes necessary for the sperm to penetrate the oocyte's coat and fertilize it [180, 181]. The head is attached to the tail via the connecting piece (also called the neck), a complex asymmetrical and segmented structure which anchors flagellar structures to the sperm cell body [182–184].

3.1.2 Middle piece

The connecting piece attaches the head to the flagellar middle piece (or mid-piece), which is the most proximal segment of the tail and is defined by the presence of the mitochondrial sheath. It contains a complete axoneme, with its typical 9+2 MT arrangement. The mitochondrial sheath contributes to the ATP production in the sperm

cell [185, 186] and it consists of mitochondrial helices wrapped around the axoneme [187]. Depending on which organism is examined, the mitochondrial sheath includes one to five helices [188] and covers between 4 µm and over 100 µm of the axoneme, with some intra-species variation as well [176]. In the middle piece, between the axoneme and the mitochondrial sheath, are also found nine outer dense fibres (ODF), which are dense, elastic structures that connect to and elongate along each axonemal dMT [189]. They extend into the next part of the sperm tail, the principal piece, where they taper and eventually terminate. The ODF improve the elasticity of the sperm flagellum, protecting it from physical damage [190] and stabilizing its axonemal structure to efficiently maintain motility [191, 192]. Each fibre differs in thickness from the others in the same flagellum, which was proposed to affect the three-dimensional wave propagation of the flagellar beat in a non-symmetrical fashion [193].

3.1.3 Principal piece

The principal piece covers most of the length of the flagellum and in the human spermatozoon it has a thickness of approximately 0.4 to 0.5 µm, even though a large variation was observed between individual cells (**Paper I**). The principal piece is defined by the presence of the fibrous sheath, which underlies the flagellar membrane and surrounds the axoneme and the outer dense fibres. The fibrous sheath is a matrix of proteins consisting of two columns that extend parallel to the axoneme and many semi-circular interlinked ribs connecting the two columns on both sides [194] (**Paper I**). This peculiar structure is proposed to limit the flexibility of the flagellum, resulting in an anisotropic beat in its more proximal part [195]. More distally, the fibrous sheath tapers and imposes a lesser restriction on the flagellum beat [175]. The fibrous sheath is also rich in signalling enzymes, important for sperm swimming, and in glycolytic enzymes, which contribute to ATP production along with the mitochondrial sheath [194].

3.1.4 End piece

The end piece is the most distal piece of the sperm tail, spanning from the end of the fibrous sheath to the distal extremity of the flagellum. It is defined by the absence of auxiliary structures as it only includes the axonemal MTs and the surrounding flagellar membrane [175, 192]. In humans, the average end piece length is about 6 µm and its thickness progressively decreases towards its distal tip (**Paper I**). The axonemal MTs lose their symmetrical arrangement as they extend into the end piece and dMTs transition into sMTs, which eventually terminate towards the distal tip [26, 104]. This region of the end piece containing sMTs is defined as the singlet region. The termination pattern of MTs is extremely variable between individual cells, causing a large morphological variability of the singlet region and the end piece altogether (**Paper I**). As the axonemal symmetry is lost in the singlet region [26], the end piece does not contribute to the flagellar beat, which was proposed to actually improve the overall propelling performance of the sperm cell [196]. The ultrastructural details of the singlet region and how the axoneme transitions into it are the focus of the next section of this chapter.

3.2 Singlet region

The singlet region is not a feature exclusive to the mammalian sperm flagellum. In fact, it is also found in model organisms such as the protists *Chlamydomonas reinhardtii* and *Tetrahymena thermophila*, where the B-tubule of each axonemal dMT terminates, while the A-tubules extend 200 to 400 nm longer, all the way to the flagellum tip [141, 197–199]. However, it isn't a universal flagellar feature either, since it is absent in other models like the kinetoplasts *Trypanosoma brucei* and *Leishmania mexicana* [97, 138, 200]. Previous observations on human sperm reported a variable number of sMTs in the singlet region, up to a total of 18 [26, 193]. This can only be accounted for if, unlike in the protist models, the B-tubules of the axonemal dMTs also extend to the tip as complete sMTs, together with the A-tubules. It is unclear whether the CP MTs also extend

into the singlet region in human spermatozoa, since they are structurally undistinguishable from sMT extensions from dMTs. However, our cryo-ET data shows that in some human spermatozoa, the CP does terminate before reaching the singlet region (**Paper II**), which might explain why a maximum number of 18 sMTs (instead of 20) has been observed at the tip.

Separation between the A- and B-tubules in one dMT has previously been described in nematode neuronal cilia [201–203] but it has never been observed directly in mammalian sperm. Such ultrastructural variability among model organisms posed the question of what the MT architecture would look like in humans specifically. This prompted us to perform cryo-ET on human and bovine spermatozoa and the results are described in **Paper I**.

3.2.1 Microtubules in the singlet region

Cryo-ET was acquired on the end pieces of 23 intact human spermatozoa on a Tecnai F30 electron microscope operated at 300 kV with a 4K CCD GATAN UltraCam detector. After the flagellar MTs were modelled in 3D, a large heterogeneity was observed regarding their number and termination patterns in the singlet region. In most instances, the plasma membrane at the end piece

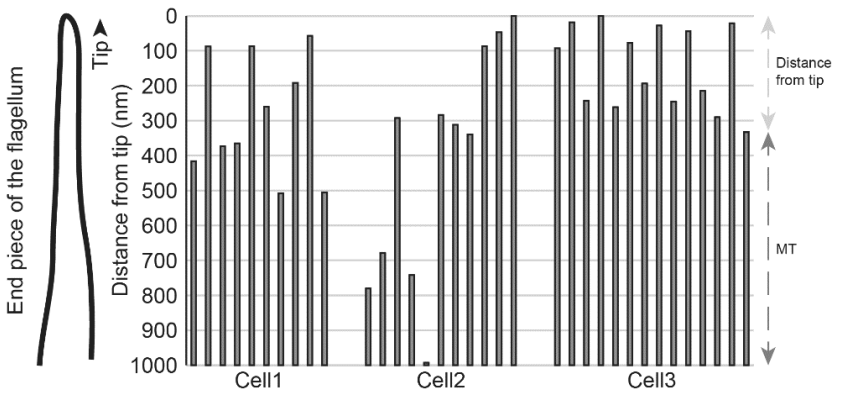

Figure 3.2: Microtubule number and termination patterns in the human sperm singlet region. The distance between the termination point and the respective flagellar tip was measured for each MT in the end pieces of three sperm cells. No termination pattern could be recognized as both MT number and termination points were highly heterogeneous. Figure reproduced with permission from **Paper I**. (https://creativecommons.org/licenses/by-nc-nd/4.0/).

accurately outlined the flagellar volume occupied by sMTs, meaning that sperm tip morphology was greatly variable as well. Three of the acquired tomograms included the distal extremity of the flagellum, which made it possible to accurately examine their MT termination patterns, measured as the distance between the MT termination points and the flagellar distal tip (Figure 3.2). No obvious pattern emerged when comparing the three end pieces, as MTs were shown to terminate as far as 1 µm from the tip, while some extended all the way to the tip. The three end pieces included a total of 10, 11 and 14 sMTs, which in the latter case exceeded the maximum of 11 sMTs expected if only the CP and the A-tubules extended into the singlet region, like in *C. reinhardtii*.

3.2.2 Transition of the axoneme into the singlet region

The investigation of a tomogram acquired 2 µm away from the tip, revealed the nature of the transition of several dMTs into the singlet region (Figure 3.3). Three different dMTs were visualized in a region qhere the A- and B-tubules separated from each other and both extended as sMTs into the singlet region. However, termination of B-tubules and extension of the respective A-tubules was also

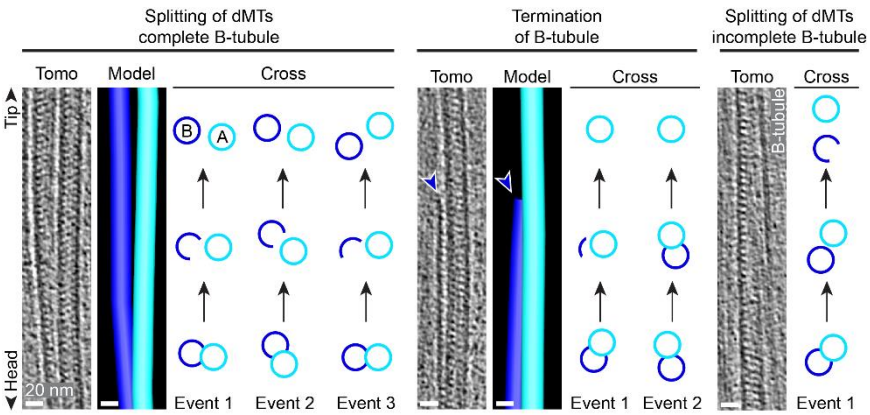

Figure 3.3: Axonemal doublet microtubules transition into the singlet region via three possible modes. The three modes are: separation of the A- (light blue) and B-tubule (dark blue) as two complete singlet MTs, termination of the B-tubule (dark blue arrowheads) and separation of the B-tubule as an incomplete MT. Each transition mode is illustrated with a longitudinal tomographic slice and illustrative model. In addition, each event is shown in a cross-view cartoon as it progresses along the MTs towards the tip. Figure reproduced with permission from **Paper I** (https://creativecommons.org/licenses/by-nc-nd/4.0/).

observed in two events, just like it was previously reported for model protists [197–199]. Finally, in a single occasion, a B-tubule was observed to separate from its A-tubule and remain an open tubulin lattice, failing to transition into a complete 13-protofilaments sMT.

Sperm end pieces with more than 11 sMTs were also observed in high-pressure frozen and plastic embedded bovine samples. The separation of A- and B-tubules and the termination of B-tubules were then directly observed in a cryo-electron micrograph of a bovine sperm tip, suggesting that transition from dMTs into two sMTs may be common among mammalian species.

These results point towards the intriguing possibility that the formation of three new protofilaments on the B-tubule is initiated *de novo* at the separation point. The cryo-ET revealed no obvious density associated to the separation point of the dMTs, which implies that the initiation of new protofilaments is either a spontaneous phenomenon or it is mediated by small or transient molecular components. In the neuronal cilia of the nematode *Caenorhabditis elegans*, the A- and B-tubules separate and reconnect based on a finely tuned post-translational polyglutamylation of the MTs [201–203]. It is entirely possible that a similar mechanism underlies the splitting of dMTs in mammalian sperm as well. Alternatively, the small [204], plus-end tracking MT-binding EB1 protein could be involved in the process. EB1 has been reported to promote 13-protofilament MT formation [205] and tubulin sheet closure [66] *in vitro*, therefore it is possible that these activities could occur *in vivo* as well.

The structure of the human singlet region revealed in **Paper I** highlights the importance of investigating the human system, as it differed from all the common model organisms used in flagellar research. Our analysis also shows that human spermatozoa is an ideal model for studying human flagellar structure using cryo-ET, as its simple and non-invasive sample preparation allows for direct visualization of the biological material in its native environment.

Chapter 4

TAILS is a sperm tip-specific microtubule inner structure

While studying the MT architecture in human sperm flagella, the cryo-EM data showed that the MTs in the end piece were decorated with an unexpected repeating feature. Cryo-ET revealed that such decoration was an interrupted helix bound to the luminal side of the MT wall. The structure was named TAILS: Tail Axoneme Intra-Luminal Spiral. TAILS is the most extensive inner MT structure described to date and the rest of this thesis will focus on illustrating its structural properties and our experimental approach to identify which protein(s) it is composed of. This chapter in particular summarizes the results presented in **Paper II**.

4.1 Localization

According to our cryo-ET data, the decoration of TAILS in tip MTs was complete, as it was found binding to the entire MT luminal wall in all three tomograms that included the distal tip. One tomogram included the transition of axonemal dMTs into sMTs, at 2.5 µm from the flagellar tip. TAILS was present in the sMTs, it extended into the A-tubules of the doublets and the B-tubules were decorated with a TAILS-like structure as well. This showed that TAILS, in at least one instance, extended in the MT lumen for as far as 3 µm from the tip. TAILS was otherwise never observed in axonemal dMTs, suggesting that it may only be present as the doublets are transitioning into singlets. However, TAILS was also found in the full axoneme, inside the CP. This was observed in three different tomograms, reaching as far from the tip as over 10 µm. While this might mean that TAILS extends longer in the CP, our observations suggest otherwise. Even though cryo-ET alone does not allow to recognize CP MTs among other MTs in the singlet region, it is likely

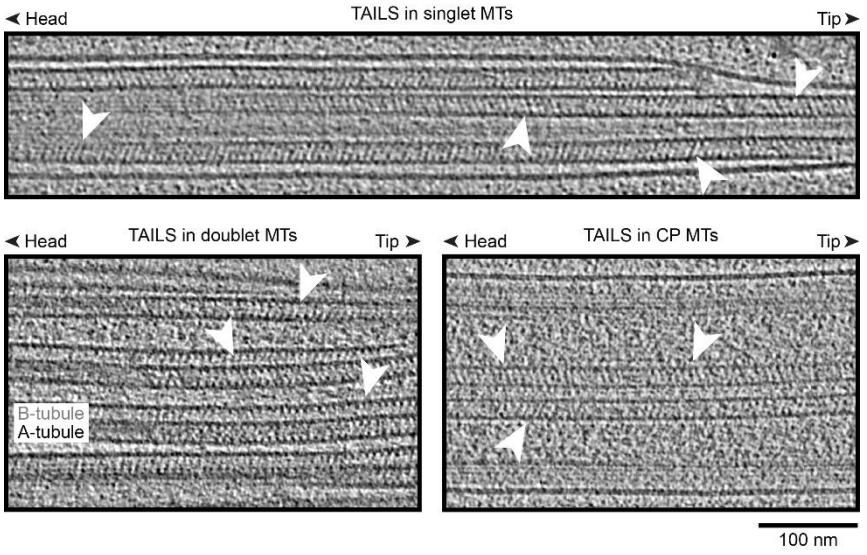

Figure 4.1: Localization of TAILS in human sperm tips. TAILS was found in the lumen of all investigated MTs in the singlet region and it was also found decorating doublets and central pair MTs.

that the CP terminates before reaching the singlet region. In fact, in one tomogram the CP was shown to terminate at 7.5 µm from the tip. Therefore, we inferred that TAILS likely binds specifically to the MT plus-end, regardless of whether it is included in the singlet region.

4.2 Ultrastructure

4.2.1 TAILS in singlet microtubules

Cryo-EM of sMTs in the human end pieces revealed that TAILS is a repeated structure with an 8 nm periodicity. A deeper insight was gained with cryo-ET and sub-tomogram averaging, which combined almost 2000 sub-volumes. The results revealed that TAILS is a left-handed interrupted helix which makes direct contact with the MT luminal wall along 11 PFs. It leaves a gap over the remaining two PFs, which corresponds to the location of the MT seam. The pitch and the handedness match those of the tubulin B-lattice, which might be an indication that the TAILS components interact with a

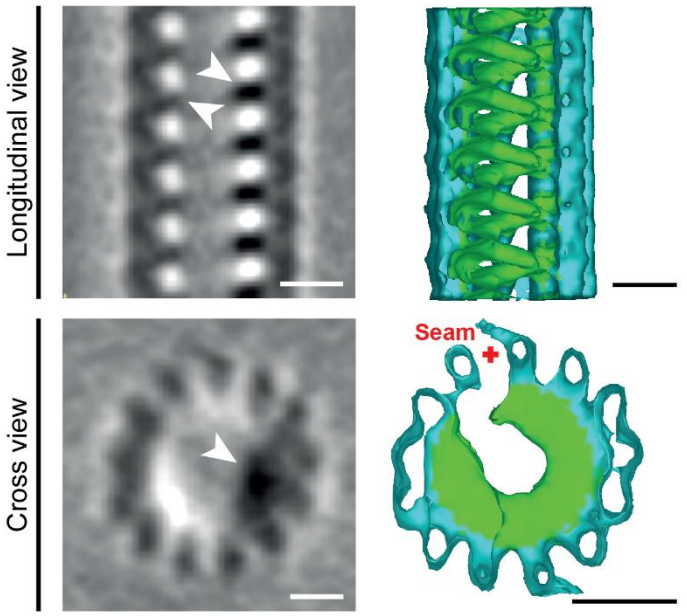

Figure 4.2: The ultrastructure of TAILS in singlet MTs. TAILS is formed by many helical segments that span over 11 PFs and leave a gap over the MT seam. Figure reproduced with changes from **Paper II** (http://creativecommons.org/licenses/by/4.0/).

specific binding site on the tubulin dimers. This would explain why TAILS is interrupted at the seam, since that is where the B-lattice of the MT is replaced with an A-lattice.

4.2.2 TAILS in doublet microtubules

The tomogram containing dMTs with TAILS was selected for sub-tomogram averaging. When averaging sMTs, the software occasionally struggles to properly rotate each particle along its longitudinal axis, as MTs are not proper helices, but rather pseudo-helices. The presence of the B-tubule in doublets helped to circumvent this problem and, although less than 500 sub-volumes were picked, the averaging process highlighted the molecular features of TAILS successfully. Its helical segments were confirmed to be present in the A-tubule lumen, with the same pitch and periodicity as in sMTs. A TAILS-like structure was present in the lumen of the B-tubules as well, although it only spanned across the inner surface of 7 or 8 PFs.

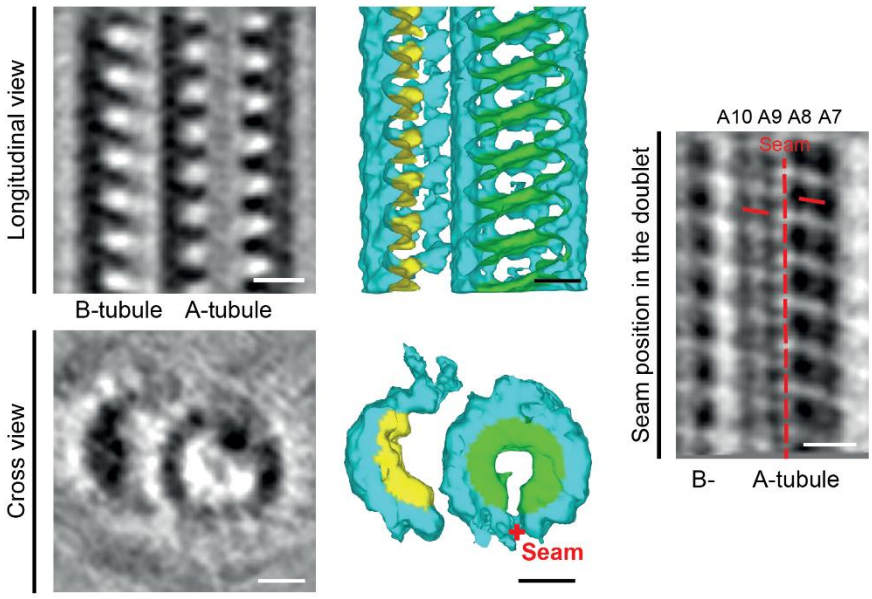

Figure 4.3: The ultrastructure of TAILS in doublet MTs. TAILS is present in the A-tubule and a TAILS-like structure is present in the B-tubule, spanning over 7-8 PFs. The position of the A-tubule seam was indirectly identified by the gap of TAILS and it was directly visualized between PFs A8 and A9. Figure reproduced with changes from **Paper II** (http://creativecommons.org/licenses/by/4.0/).

The doublet average had an anisotropic resolution since the dMTs included in the analysis were similarly oriented in space. However, some PFs reached a resolution high enough to make out individual tubulin monomers. This allowed us to visualize the attachment site of TAILS to tubulin, which appeared to be located between subunits, rather than directly onto the α- or β-subunit.

The gap left between TAILS segments in the doublet's A-tubule aligned with the position between PFs A8 and A9, on the outer side of the doublet. The sub-tomogram averaging of singlets confirmed it as the seam position, since the tubulin lattice was visible in the doublet average and the seam could be visualized directly. This seam position is not in agreement with previously published ones, however these previous studies focused on organisms other than human, such as sea urchin (seam between PFs A1 and A2) [31] and *Tetrahymena thermophila* [84, 206]. It is possible that the reported

structural discrepancies reflect biological differences between species.

4.2.3 Models for TAILS molecular structure

Based on this dataset, it is not possible to distinguish whether each helical segment of TAILS is composed of a single large protein or separate monomers, therefore **Paper II** presented both models as equally valid. In the latter case, it would be possible that one helical segment was made up of 11 subunits, each binding to one PF. This hypothesis assumes that TAILS interacts with tubulin on a specific binding site and that this binding site is disrupted at the seam. The fact that a shorter TAILS-like structure is found in B-tubules suggests that the second model might be the more accurate one, where some monomers associate with tubulin but others do not due to steric hindrance. This model is discussed further in **Paper III**, where a higher resolution structure of TAILS is presented.

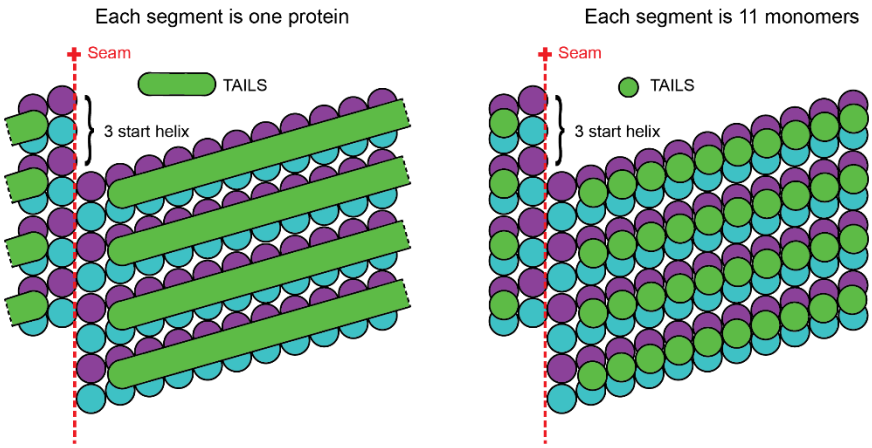

Figure 4.4: Two models proposed for the structure of TAILS. In **Paper II** we proposed that each helical segment of TAILS could be made up of a single large protein or by 11 monomers, each one binding at an interface between two tubulin subunits. Figure reproduced from **Paper II** (http://creativecommons.org/licenses/by/4.0/).

4.3 Proposed functions of TAILS

The fact that TAILS is such a dominant feature in sperm tip MTs suggests that it performs an important function, with either a structural role, a physiological role or both. The following hypotheses are presented and the real function of TAILS may very well be a combination of two or all of them.

1) Since TAILS binds to MTs towards their plus-end, it may be involved in regulating their dynamic instability. The energetic cost of constantly growing and shrinking MTs would likely not be affordable for a sperm cell, whose energy needs to be focused on its only goal of reaching and fertilizing the egg. Additionally, there is no active flagellar transport in mature mammalian spermatozoa [207], which means that fresh GTP-tubulin would have to diffuse all the way to the sperm tip for polymerization. TAILS might bind to MTs to stabilize their structure by preventing depolymerization and thus helping the cell focus its energy on swimming rather than on MT dynamics.

2) TAILS might affect the stiffness of the MTs in the end piece, therefore affecting the swimming efficiency of the spermatozoon. No molecular motors are found in the singlet region [26], meaning that the MTs at the flagellar tip do not contribute to the flagellar beat. However, a non-beating end piece was shown to improve cell propulsion in computational simulations [196] and stiff MTs might enhance this effect. This hypothesis is supported by studies suggesting that the end piece has a different stiffness compared to the rest of the flagellum [208] and that most of the beating energy is released in the distal part of the flagellum [209].

3) One final hypothesis is that TAILS binds to MTs to induce changes in the tubulin lattice, similarly to how hydrolysis of GTP in β-tubulin leads to a lattice compaction [12]. A tip-specific lattice is an intriguing possibility (as previously presented in [67]), since it could enable binding of tip-specific proteins, while excluding other axonemal MAPs. Tip-specific proteins could be involved in signalling pathways and in MT homeostasis. A

similar decoration to TAILS was observed in the transition zone of bovine tracheal flagella, but not in their basal body or axonemal MTs [92]. This supports the idea that extensive MIPs like TAILS might help the cell define functional compartments along its flagella.

In order to test these hypotheses, the biochemical properties of TAILS need to be assessed *in vitro* and *in vivo*, if it were possible to observe the phenotype of a potential deletion mutant. The identification of the protein, or proteins, that make up TAILS is therefore a priority. **Paper III**, discussed in the next chapter, illustrates the progress of our current approach.

Chapter 5

Identifying TAILS

Structural biology is typically carried out following a conventional workflow: a protein of interest is identified, then purified and prepared for high-resolution studies to determine its structure (for example using X-ray crystallography or cryo-EM). However, a reverse approach to structural biology, where an unknown protein is first visualized as an electron density and then purified and identified, poses a new challenge. This chapter discusses the work presented in **Paper III**, a manuscript in preparation where we identify TAILS candidate proteins based on a multi-pronged approach (Figure 5.1):

1) Since TAILS is highly concentrated in sperm end pieces, we used comparative proteomics to identify proteins enriched at the flagellar tip compared to the rest of the tail.

2) Cryo-ET data of flagellar tips from different species was acquired to investigate how conserved TAILS is across evolution. This information was then combined with the sperm tip proteome to form a candidate list by excluding proteins with homologues in organisms without TAILS.

3) In addition, we reconstructed a high-resolution map of TAILS by cryo-EM single particle analysis, with the intent of revealing its secondary structure, or even aminoacidic residues, to directly identify its components, as it's been achieved for other proteins [210].

4) Finally, once a handful of candidates are selected, they can be individually characterized structurally and biochemically. In this thesis, preliminary work on the candidate protein DCDC2C is discussed.

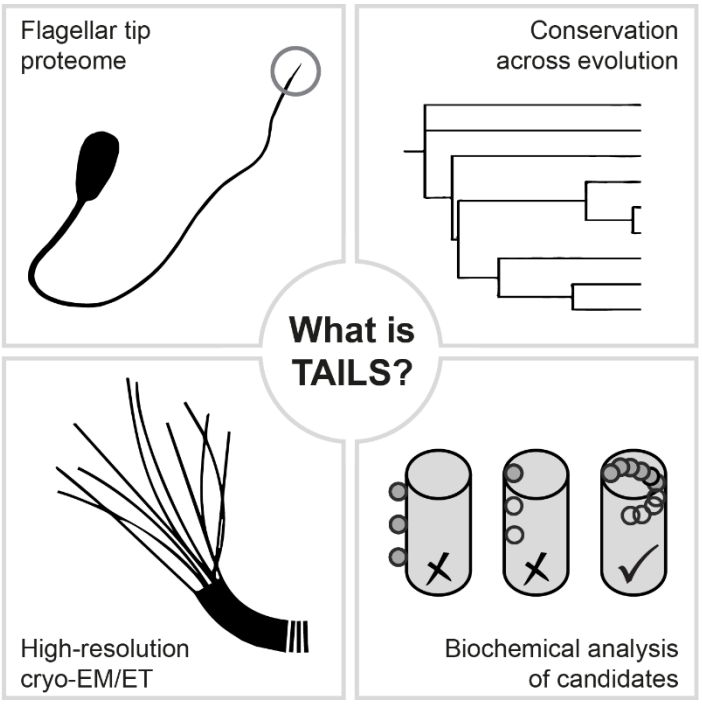

Figure 5.1: Schematic representation of the multi-pronged approach designed to identify TAILS. 1) A sperm tip proteome was obtained. 2) The conservation of TAILS among different species was investigated with cryo-ET. 3) High-resolution structures of TAILS were reconstructed with single particle analysis from splayed tips (shown in the diagram) and with sub-tomogram averaging from intact tips. 4) Candidates and their interaction with MTs are being biochemically characterized.

5.1 Sperm tip proteome

Proteomics information on sperm cells, and specifically on sperm flagella, is already available in the literature [211–216]. While TAILS is possibly represented in this data, it is likely a non-abundant hit, as it is exclusively localized at the sperm tip (~ 3 µm long) and proteins associated with the axoneme (~ 50 µm long) are present in overall much higher amounts. Since each of these studies presents hundreds of proteins associated with the sperm cell and its flagellum, looking for TAILS in these datasets would be a hunt for a needle in a haystack. For this reason, we developed several protocols to obtain a sample of enriched sperm tips that could be used for proteomics analysis. In our workflow, sperm cells were

physically fragmented (either selectively by laser dissection or randomly by sonication) and the tip fragments were separated or enriched based on their physical or biochemical properties. Due to limitations in obtaining human samples, these experiments were instead performed on bovine sperm, which is a valid model since we confirmed it also contains TAILS (see section 5.2.1). It also had the benefit that all human protein contamination in the samples could easily be excluded.

5.1.1 Laser dissection

The first attempt at purifying sperm tips involved laser dissection, which allows to selectively excise and collect parts of a sample as it's been visualized with an optical microscope (Figure 5.3). The instrument used was a Zeiss Axio observer Z1 equipped with a PALM MicroBeam system. The sample is prepared on a glass slide coated with a sticky membrane, which the cells adhere to. The laser is then targeted to dissect the membrane around an area of interest, which can include sub-cellular fragments, and then catapult the dissected area upwards into a collection tube with a laser pulse. A

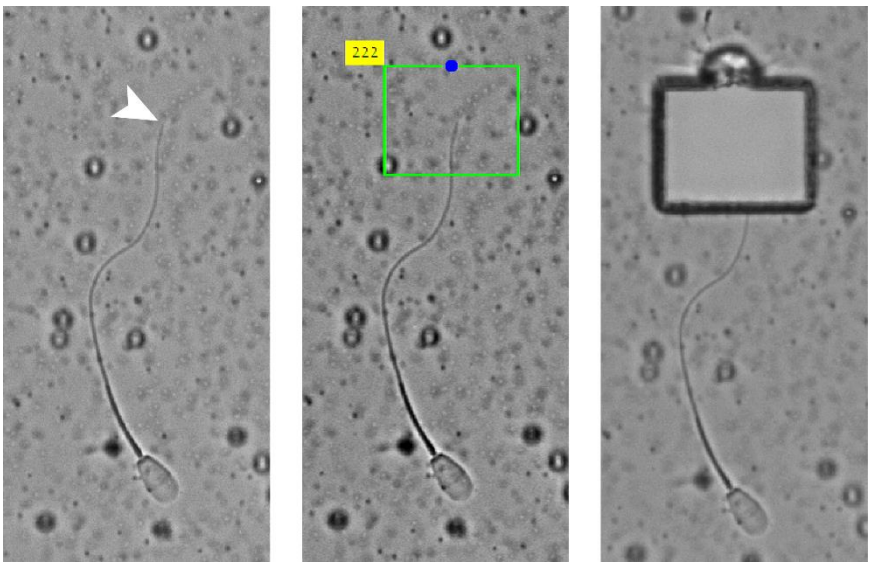

Figure 5.2: Laser dissection of bovine sperm tips. As the sperm cells are adhering to a sticky membrane, the flagellum end piece (arrowhead) is selected and then catapulted upwards for collection.

total of over 8000 sperm tips were collected, which together are approximately equivalent to only 1.44% of the entire volume of a single, small eukaryotic cell with a diameter of 10 µm (assuming the tip volume is a 3 µm-long cylinder with a radius of 100 nm). Likely due to the small size of the sample, the proteomics results from this experiment were inconclusive, as contaminating proteins were dominating the dataset. Therefore, other collection methods were explored.

5.1.2 Sonication

A sonication protocol was optimized (adapted from [217]) as a non-specific segmentation method. After being washed in 1x PBS three times, bovine sperm cells were sonicated for 10 seconds between 1 and 8 times. The sonication was carried out to break the cells into fragments of variable size, with the intention of separating the tip fragments from the rest of the cell debris in the successive steps (Figure 5.3). Negative staining EM was performed on the sonicated cells and the number of intact tip fragments was quantified for each condition. Sonicating only once was sufficient to fragment the cells successfully and yielded the highest number of intact tips, preventing excessive damage.

5.1.3 Density gradients

The sonicated sperm cells were loaded onto two consecutive sucrose-based density gradients to separate the lighter fragments like the tips from the denser fragments like the heads and mitochondria (Figure 5.3). The first gradient (20-60-80% density layers), performed as in [218], was sufficient to separate the tips (floating above 60%) from the heads (pelleting under 80%), however the tips fraction was run on a second gradient (20-55-60-65-70-80%) to wash away contaminating membrane debris. Negative staining EM was used to quantify the tip enrichment (Figure 5.3). In each experiment, tips and necks (connecting pieces, representing non-tip material) were quantified over 5 grid squares and their ratio was calculated for every collected fraction. Pairs of most and least enriched fractions, with an enrichment by at least a

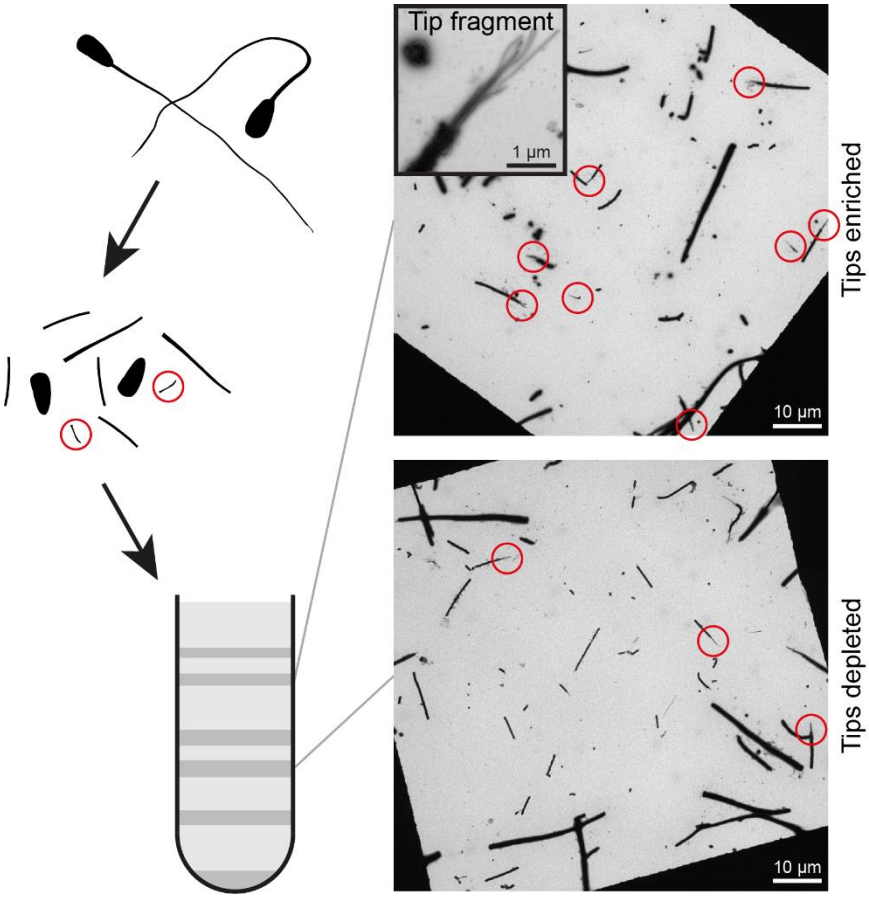

Figure 5.3: Workflow of enrichment for flagellar tips. Washed, intact sperm cells were fragmented via sonication and tips fragment were enriched in sucrose density gradients. The enrichment was quantified with negative staining EM of the collected fractions.

factor of 2, were selected from four experimental replicates and sent for comparative mass spectrometry.

5.1.4 FACS sorting

As an alternative to a density-based enrichment, we are exploring the possibility of sorting tip fragments with FACS (fluorescence-activated cell sorting) by using a tip-specific fluorescent marker. In the FACS machine, cell fragments are flowing in a stream of small electrically charged droplets. The fluorescence signal of each droplet is detected and its trajectory can be altered using a targeted

electrical field, which allows for sorting of differently fluorescent fragments [219].

An sperm tip marker was identified in DCDC2C, a small protein that was reported to specifically localize to the end piece of human spermatozoa [220]. Immuno-fluorescence experiments have been successful in replicating the tip-specific signal (Figure 5.4) and a protocol for FACS enrichment is currently under development.

5.1.5 Mass spectrometry of sperm tips

Mass spectrometry is a sensitive technique which can accurately identify the proteins present in a biological sample [221]. During preparation, the sample is homogenized and proteins are lysed into short peptides. Each protein will produce unique and overlapping peptides based on its individual amino-acidic sequence. When the experiment is run in the mass spectrometry machine, peptides are ionized and inserted into a magnetic trap, where they oscillate in different ways depending on their mass and charge [222]. The changes in oscillations are recorded and can be accurately used to calculate each peptide's mass, which is directly dependent on its

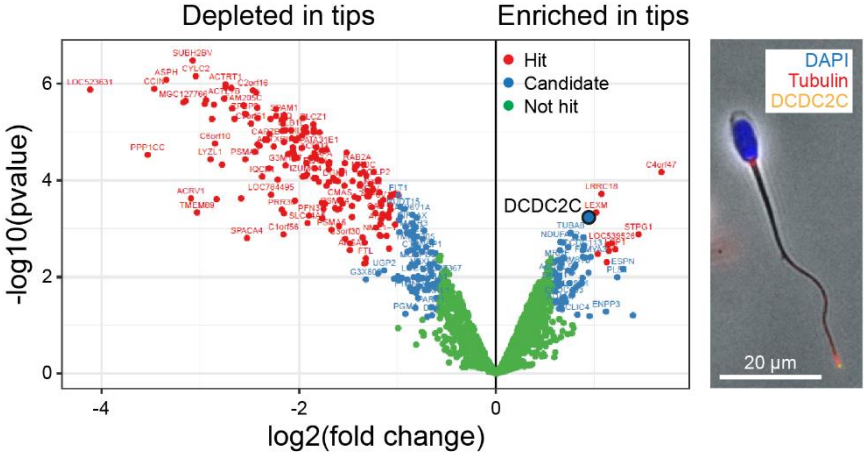

Figure 5.4: Mass spectrometry analysis identified proteins enriched in the tips. The volcano plot shows hit and candidate proteins, defined based on fold enrichment and statistical significance. Among them was DCDC2C, which is not only a sperm tip marker, but also a potential candidate for TAILS. On the right, immunofluorescence reveals the localization of DCDC2C.

sequence. When run against a database of known protein sequences, the protein content of the sample is revealed.

In the experiment presented in this thesis, the protein content of a tip-enriched fraction was compared to a non-enriched control. This was done by labelling the two samples with chemical tags of different mass so that they can be distinguished from each other [223]. The number of peptides identified for the same protein in either sample gives a quantitative ratio of its content. The results yielded the first, to our knowledge, flagellar tip proteome (Figure 5.4), which included 70 proteins showing a significant enrichment of at least 50% in the tips fraction compared to the control fraction. The tip marker DCDC2C discussed earlier was identified as enriched in the tips, supporting the validity of the data. Its flagellar localization was confirmed by our own immuno-fluorescence experiment (Figure 5.4), making DCDC2C a putative candidate to be a TAILS protein itself.

5.2 TAILS across evolution

Many of the hits identified by mass spectrometry are uncharacterized proteins, which would require unreasonable time and resources to be investigated individually. Therefore, we decided to explore the presence of TAILS in organisms other than humans. We selected fully sequenced and well annotated models that are evolutionarily distant from one another, so that we could look for homologues of our proteomics hits in their genomes.

5.2.1 Cryo-ET of flagellar tips in different species

Sperm samples from cattle (*Bos taurus*), chicken (*Gallus gallus domesticus*) and frog (*Xenopus tropicalis*) were plunge-frozen and cryo-ET was performed on the flagellar tips to reveal the presence or absence of TAILS. In addition, previously acquired cryo-ET data of *T. brucei* and published data on *C. reinhardtii* [141] were included in the analysis. All investigated animals showed presence of TAILS in sperm tips, while it was absent in the examined protists (Figure 5.5).

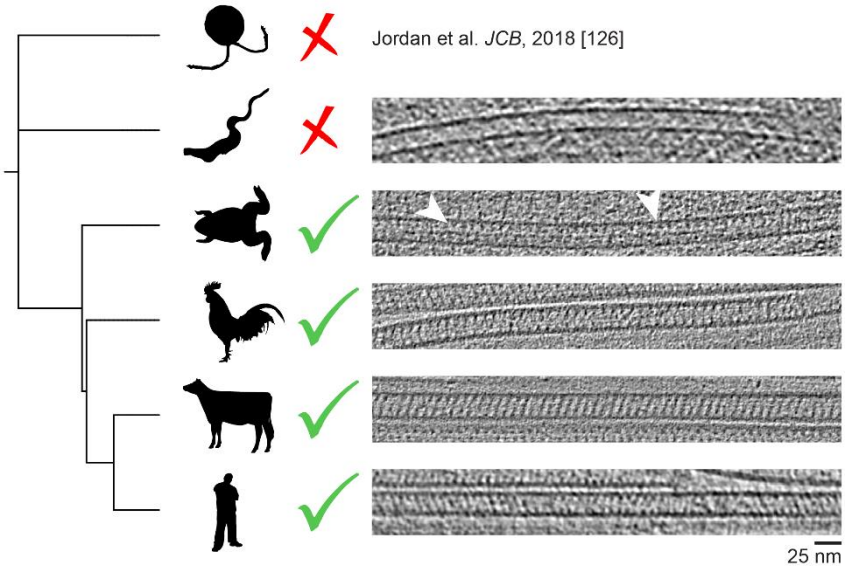

Figure 5.5: Conservation of TAILS among the investigated organisms. After its discovery in humans, the presence of TAILS was confirmed by cryo-ET in bovine, chicken and frog. TAILS was absent in trypanosomes and in *C. reinhardtii* as well, as can be seen from cryo-ET of the flagellar tip in [126].

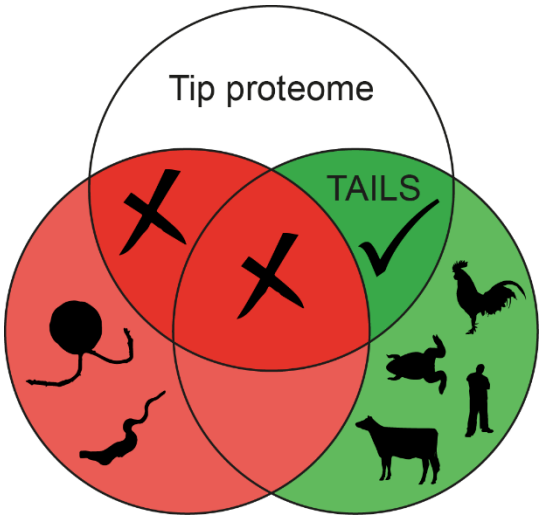

Figure 5.6: Venn diagram illustrating the approach applied to shorten the candidate list. Candidates from the bovine tip proteome were discarded if they did not have homologues in human, frog and chicken or if they have homologues in trypanosomes or *C. reinhardtii*. Candidates with homologues in animals but not in protists will be investigated further.

5.2.2 Narrowing down TAILS candidates

The information gathered from the different species could be used to shorten the list of TAILS candidates obtained from the proteomics experiment. Since all investigated organisms are fully sequenced and well annotated, the gene names of the protein hits could be easily found in bovine and run on BLAST [224] to look for homologous genes in the other organisms. Plausible candidates from bovine would only have homologs in human, chicken and frog and none in the two protists. Therefore, any candidate following a different pattern was discarded (Figure 5.6). The final list counted a total of 20 proteins, including DCDC2C. This method is assuming that the proteins forming TAILS do not have an alternative localization in the two protists, which is a limitation of our approach.

5.3 High-resolution structure of TAILS

Thanks to the recent advances in cryo-EM, it has become possible to reconstruct high-resolution protein structures showing secondary structures or even residue side chains. These structural details can be sufficient to successfully identify a previously unknown protein purely based on microscopy data [87, 98, 210]. In the hopes of achieving such results, we developed a protocol to demembranate the human sperm flagellum tip without depolymerizing the internal microtubules and performed single particle cryo-EM of TAILS in these splayed tips. Sub-tomogram averaging of TAILS was also performed on a new cryo-ET dataset acquired on bovine, improving on the previous structure which was recorded before direct electron detectors were available.

5.3.1 Sub-tomogram averaging with PEET

Cryo-ET was performed on intact bovine sperm tips on a state-of-the-art Titan Krios cryo-electron microscope equipped with a direct electron detector (K2 camera). The MTs in the singlet region of sperm tips were modelled in the 10 best tomograms and a new sub-tomogram average was calculated with PEET (Figure 5.7). The tubulin monomers were clearly visible along the PFs and so was

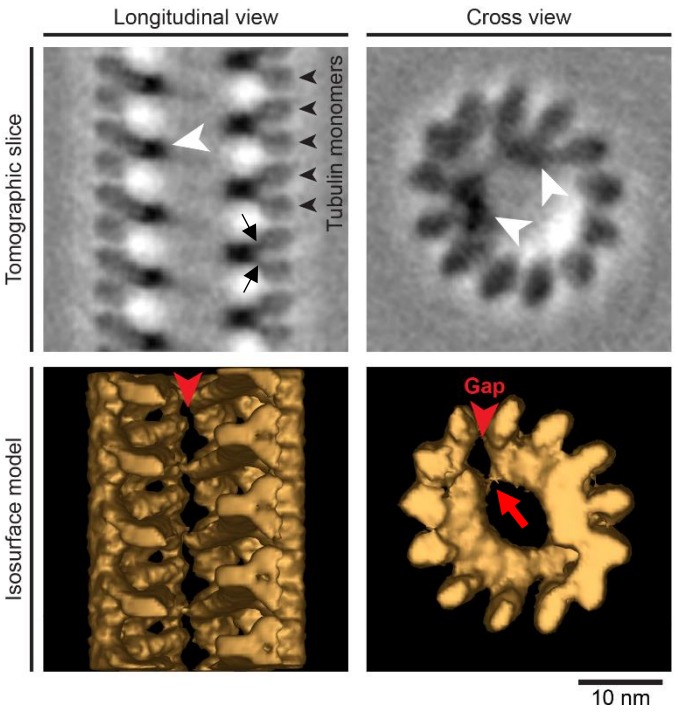

Figure 5.7: Improved sub-tomogram averaging of TAILS in bovine. The new dataset offered new insight into the structure of TAILS (white arrowheads), revealing the details of its attachments (black arrows) to tubulin (black arrowheads) and a possible bridge (red arrow) over the gap (red arrowhead).

TAILS, which was now confirmed to bind at the interface between two adjacent tubulin monomers. String-like connections could be seen attaching TAILS to each of the two monomers (Figure 5.7, small black arrows). A faint connection appeared to exist over the gap between two consecutive TAILS segments, suggesting that it might be a flexible bridge structure that is hardly resolved by averaging. As shown in the cross-view of the isosurface model, the volume of TAILS does not seem to occupy an even amount of luminal space along the entire segment, as TAILS appears thinner opposite to its gap. This indicates that TAILS may not be composed of identical monomers. More insight on this was offered by cryo-EM single particle analysis.

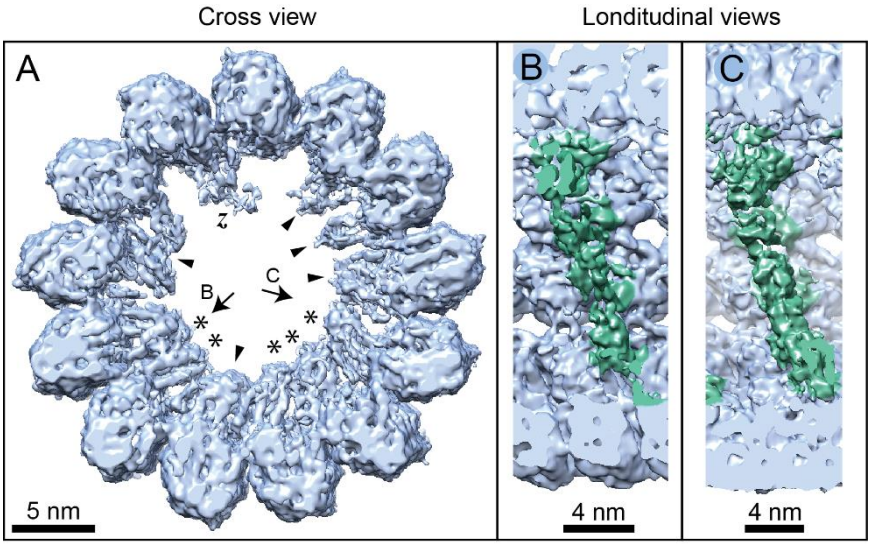

Figure 5.8: Single particle analysis of TAILS in splayed MTs. A) The density map revealed potentially up to 6 different protein densities in TAILS (5 arrowheads + identical copies of asterisk). In addition, a novel zipper density (z) with a periodicity of 4 nm was discovered in the TAILS gap. B-C) Side views of TAILS as indicated in panel A.

5.3.2 Single particle analysis on sperm tip microtubules

Single particle analysis requires that during data acquisition the structure of interest does not overlap with other structures which interfere with particle picking and introduce noise in the reconstruction. For this reason, such analysis could not be performed on intact cell tips, where MTs are tightly packed inside the flagellar membrane. Human sperm end pieces were demembranated with a mild detergent treatment (0.25% Triton X-100 in HBSS supplemented with 50 mM KCl and 1 mM PMSF for 20 minutes), which allowed the sMTs to splay apart in solution with minimal overlapping. The sample was then applied to EM grids and plunge frozen for single particle data acquisition.

Data is still being analysed at the moment of writing this thesis (approximately 45000 particles picked so far), however preliminary results show remarkable and unprecedented detail of the structure of TAILS at an estimated resolution of ~ 6.5 Å (Figure 5.8). While no protein has been identified yet from the density map, the resolution is good enough to distinguish that TAILS is likely made up of

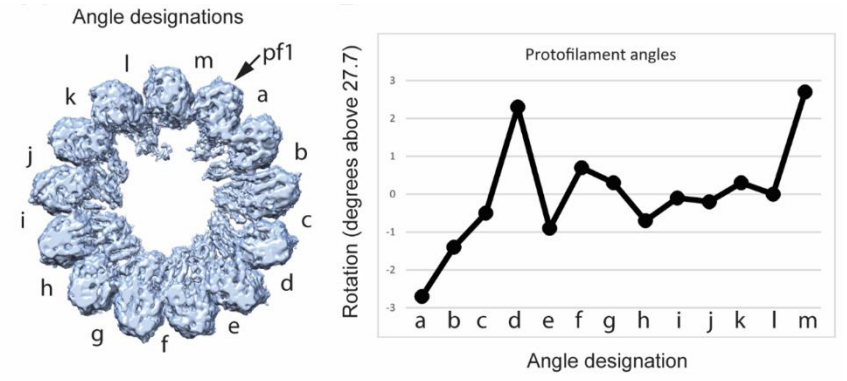

Figure 5.9: Protofilament angles in MTs with TAILS. The angles between PFs averaged at 27.7°. The biggest difference was observed at angles 1 and 13, indicating some degree of torsion of the PF in between.

multiple proteins, rejecting both structural models that were proposed in **Paper II**. We estimate that TAILS could be composed of up to 6 different proteins, one of which appears to be present in 5 copies per TAILS segment (Figure 5.8A, arrowheads and asterisks). An additional density with a periodicity of 4 nm (instead of TAILS's 8 nm repeat) was identified at the gap that TAILS leaves over the MT seam. This density was named "the zipper" and it does not appear to make direct contact with TAILS.

Additionally, the angle between each protofilament was measured, revealing some striking variability (Figure 5.9). Most angles measured around the average value of 27.7°, however angles "a" and "m" deviated from it with almost 3° in either direction, respectively. This suggests a torsion of the PF located in between these angles. Additionally, angle 4 showed an increase of over 2° as well. Similar differences have already been reported in MTs [84] and MAPs like kinesin-I as well as a GDP lattice have been shown to rotate PFs at the seam [67]. In accordance with your previous data in **Paper II**, the seam was indeed observed in position "m" (data not shown), indicating that the increased angle between PFs might be caused by a GDP state, supporting the hypothesis that sperm tip microtubules are not dynamic, or by TAILS itself.

5.4 Evaluation of candidate protein DCDC2C

DCDC2C is the first protein to be found to exclusively localize to the sperm flagellum tip [220], which is supported by our proteomics data (Figure 5.4). It also contains a doublecortin domain, which is known to bind to MTs [64], and sub-tomogram averaging revealed no obvious densities on the outer wall of tip MTs. For these reasons, DCDC2C is a potential TAILS candidate and we investigated its interaction with MTs and free tubulin.

To evaluate DCDC2C biochemically, a GFP-fusion construct was created and purified. Its interaction with MTs was assessed by TIRF (Total Internal Reflection Fluorescence) microscopy. TIRF is a powerful optical microscopy technique that selectively excites fluorophores located closest to the cover-glass, instead of the entire sample volume [225]. This gives a signal of much higher quality as it removes background fluorescence. When DCDC2C is added *in vitro* to polymerized MTs attached to the cover-glass surface, a clear co-localization was observed, indicating that DCDC2C likely has binding affinity to the MT lattice (Figure 5.10A). However, when DCDC2C was added to actively polymerizing MTs, it aggregated with free tubulin (Figure 5.10A).

To test whether this aggregation was caused by DCDC2C binding to free tubulin, a bio-layer interferometry (BLI) assay was performed [226]. In this assay, a sensor measures the thickness of biological material on its surface. When it is coated with a probe, binding of an interaction partner can be measured as an increase in average thickness. The sensor was coated with DCDC2C and its interaction with free tubulin was assessed. No change in thickness was observed after adding tubulin to the sample, indicating that DCDC2C unlikely binds to tubulin outside of the MT lattice.

As DCX is a close homologue to DCDC2C, the published structure of its C-terminal MT binding domain [227] was docked into the TAILS densities revealed by cryo-EM single particle analysis. A reasonable fit was found for the TAILS component present in

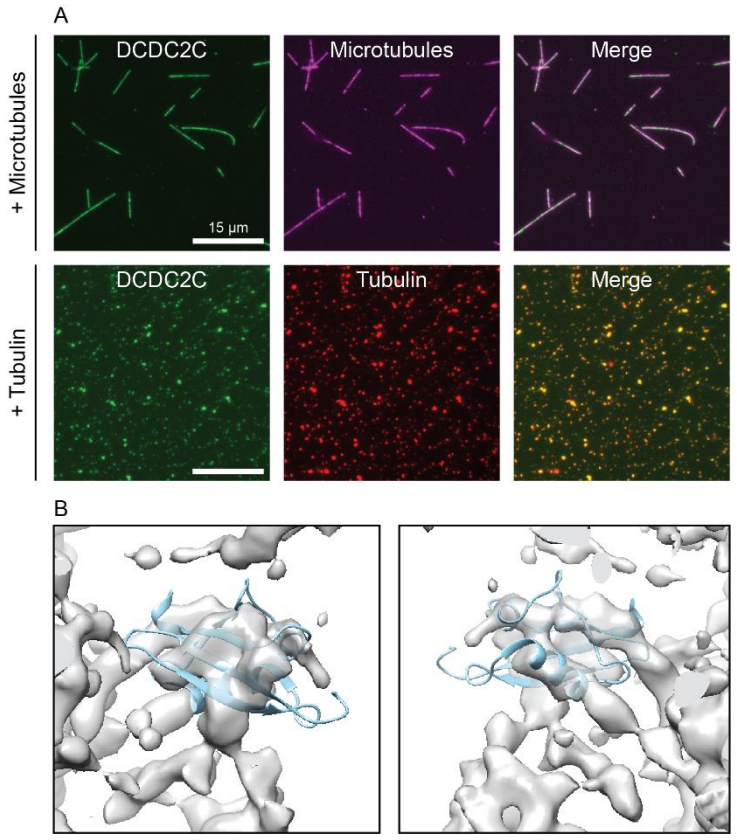

Figure 5.10: DCDC2C is a likely TAILS candidate. A) TIRF microscopy reveals that DCDC2C binds to microtubules, however it aggregates with free tubulin. B) The C-terminal MT binding domain of DCX, close homologue to DCDC2C, has a decent fit in the repeated protein density of TAILS.

multiple copies (Figure 5.10B), supporting the hypothesis that DCDC2C is a TAILS protein.

While DCDC2C is a promising TAILS candidate, these results alone are still inconclusive and more in-depth analyses must be performed to characterize the interaction that DCDC2C has with MTs. Cryo-ET of its association to MTs *in vitro*, for instance, would shed light on the location of the binding site and reveal whether it is on the luminal side. However, if DCDC2C is indeed one of the components that make up TAILS, it remains unknown whether it can bind to the inner MT wall independently from the other TAILS proteins.

Concluding summary

The work in this thesis presents a detailed insight into the ultrastructure of the human sperm end piece. First, it was illustrated how the architecture of human flagellum differs from common organisms at the distal tip, revealing high heterogeneity between sperm cells and multiple transition modes of dMTs into sMTs (**Paper I**). TAILS, an extensive inner MT decoration, was discovered and described by cryo-ET, posing the question of what function it performs and what components it is made of (**Paper II**). A multi-pronged approach was designed to address these questions (**Paper III**) and a high-resolution structure of TAILS was produced by cryo-EM single particle analysis, revealing that TAILS is made of at least 6 different components. The first, to our knowledge, flagellar tip proteome was produced, identifying 70 proteins enriched at the sperm tip. TAILS was also observed by cryo-ET in spermatozoa of bovine, chicken and frog, but not in flagellar tips of trypanosomes and *C. reinhardtii*. This information was combined with the proteomics data to compile a list of 20 candidate TAILS proteins. Among them, DCDC2C was identified as the only reported protein to exclusively localize to the human sperm tail tip. Further investigation revealed that it interacts with MTs and that it is a possible fit into the density map of one of the TAILS components revealed by single particle analysis.

These studies show the importance of investigating cellular structures in their native state, for which cryo-ET is an ideal technique of choice. A reverse structural biology approach was adopted to identify unknown structures revealed by cryo-ET. Current work is focusing on improving the resolution of our sub-tomogram average and single particle structures of TAILS and future experiments will verify if DCDC2C is indeed a TAILS protein and which other candidates are potential hits.

Bibliography

1. Harris P (1962) Some structural and functional aspects of the mitotic apparatus in sea urchin embryos. J Cell Biol 14:475–487. https://doi.org/10.1083/jcb.14.3.475
2. Roth LE, Daniels EW (1962) Electron microscopic studies of mitosis in amebae II. The giant ameba *Pelomyxa carolinensis*. J Cell Biol 12:57–78. https://doi.org/10.1083/jcb.12.1.57
3. Ledbetter MC, Porter KR (1963) A "microtubule" in plant cell fine structure. J Cell Biol 19:239–250. https://doi.org/10.1083/jcb.19.1.239
4. Slautterback DB (1963) Cytoplasmic microtubules: I. Hydra. J Cell Biol 18:367–388. https://doi.org/10.1083/jcb.18.2.367
5. Nogales E, Wolf SG, Downing KH (1998) Structure of the αβ tubulin dimer by electron crystallography. Nature 391:199–203. https://doi.org/10.1038/34465
6. Löwe J, Li H, Downing KH, Nogales E (2001) Refined structure of αβ-tubulin at 3.5 Å resolution. J Mol Biol 313:1045–1057. https://doi.org/10.1006/jmbi.2001.5077
7. Vemu A, Atherton J, Spector JO, et al (2017) Tubulin isoform composition tunes microtubule dynamics. Mol Biol Cell 28:3564–3572. https://doi.org/10.1091/mbc.e17-02-0124
8. Roll-Mecak A (2020) The Tubulin Code in Microtubule Dynamics and Information Encoding. Dev Cell 54:7–20. https://doi.org/10.1016/j.devcel.2020.06.008
9. Nogales E, Whittaker M, Milligan RA, Downing KH (1999) High-Resolution Model of the Microtubule. Cell 96:79–88. https://doi.org/10.1016/S0092-8674(00)80961-7
10. Mitchison T, Kirschner M (1984) Dynamic instability of microtubule growth. Nature 312:237–242. https://doi.org/10.1038/312237a0
11. Horio T, Hotani H (1986) Visualization of the dynamic instability of individual microtubules by dark-field microscopy. Nature 321:605–607. https://doi.org/10.1038/321605a0
12. Zhang R, Alushin GM, Brown A, Nogales E (2015) Mechanistic Origin of Microtubule Dynamic Instability and Its Modulation by EB Proteins. Cell 162:849–859. https://doi.org/10.1016/j.cell.2015.07.012
13. Alushin GM, Lander GC, Kellogg EH, et al (2014) High-Resolution Microtubule Structures Reveal the Structural Transitions in αβ-Tubulin upon GTP Hydrolysis. Cell 157:1117–1129. https://doi.org/10.1016/j.cell.2014.03.053
14. Erickson HP (1974) Microtubule surface lattice and subunit structure and observations on reassemly. J Cell Biol 60:153–167. https://doi.org/10.1083/jcb.60.1.153

15. Chrétien D, Wade RH (1991) New data on the microtubule surface lattice. Biol Cell 71:161–174. https://doi.org/10.1016/0248-4900(91)90062-R
16. Weisenberg RC (1972) Microtubule Formation in vitro in Solutions Containing Low Calcium Concentrations. Science 177:1104–1105. https://doi.org/10.1126/science.177.4054.1104
17. Olmsted JB, Borisy GG (1975) Ionic and nucleotide requirements for microtubule polymerization in vitro. Biochemistry 14:2996–3005. https://doi.org/10.1021/bi00684a032
18. Wade RH, Chrétien D (1993) Cryoelectron Microscopy of Microtubules. J Struct Biol 110:1–27. https://doi.org/10.1006/jsbi.1993.1001
19. Chrétien D, Metoz F, Verde F, et al (1992) Lattice defects in microtubules: protofilament numbers vary within individual microtubules. J Cell Biol 117:1031–1040. https://doi.org/10.1083/jcb.117.5.1031
20. Binder LI, Rosenbaum JL (1978) The in vitro assembly of flagellar outer doublet tubulin. J Cell Biol 79:500–515. https://doi.org/10.1083/jcb.79.2.500
21. Moores CA, Perderiset M, Francis F, et al (2004) Mechanism of Microtubule Stabilization by Doublecortin. Mol Cell 14:833–839. https://doi.org/10.1016/j.molcel.2004.06.009
22. Chaaban S, Brouhard GJ (2017) A microtubule bestiary: structural diversity in tubulin polymers. Mol Biol Cell 28:2924–2931. https://doi.org/10.1091/mbc.e16-05-0271
23. Chalfie M, Thomson JN (1982) Structural and functional diversity in the neuronal microtubules of *Caenorhabditis elegans*. J Cell Biol 93:15–23. https://doi.org/10.1083/jcb.93.1.15
24. Chaaban S, Jariwala S, Hsu C-T, et al (2018) The Structure and Dynamics of C. elegans Tubulin Reveals the Mechanistic Basis of Microtubule Growth. Dev Cell 47:191-204.e8. https://doi.org/10.1016/j.devcel.2018.08.023
25. Witman GB, Carlson K, Rosenbaum JL (1972) Chlamydomonas flagella : II. The distribution of tubulins 1 and 2 in the outer doublet microtubules. J Cell Biol 54:540–555. https://doi.org/10.1083/jcb.54.3.540
26. Afzelius BA, Dallai R, Lanzavecchia S, Bellon PL (1995) Flagellar structure in normal human spermatozoa and in spermatozoa that lack dynein arms. Tissue Cell 27:241–247. https://doi.org/10.1016/S0040-8166(95)80044-1
27. Zheng Y, Wong ML, Alberts B, Mitchison T (1995) Nucleation of microtubule assembly by a γ-tubulin-containing ring complex. Nature 378:578–583. https://doi.org/10.1038/378578a0
28. Moritz M, Braunfeld MB, Sedat JW, et al (1995) Microtubule nucleation by γ-tubulin-containing rings in the centrosome. Nature 378:638–640. https://doi.org/10.1038/378638a0
29. Kollman JM, Polka JK, Zelter A, et al (2010) Microtubule nucleating γ-TuSC assembles structures with 13-fold microtubule-like symmetry. Nature 466:879–882. https://doi.org/10.1038/nature09207

30. Sosa H, Milligan RA (1996) Three-dimensional Structure of ncd-decorated Microtubules Obtained by a Back-projection Method. J Mol Biol 260:743–755. https://doi.org/10.1006/jmbi.1996.0434
31. Song YH, Mandelkow E (1995) The anatomy of flagellar microtubules: polarity, seam, junctions, and lattice. J Cell Biol 128:81–94. https://doi.org/10.1083/jcb.128.1.81
32. McIntosh JR, Morphew MK, Grissom PM, et al (2009) Lattice Structure of Cytoplasmic Microtubules in a Cultured Mammalian Cell. J Mol Biol 394:177–182. https://doi.org/10.1016/j.jmb.2009.09.033
33. Kikkawa M, Ishikawa T, Nakata T, et al (1994) Direct visualization of the microtubule lattice seam both in vitro and in vivo. J Cell Biol 127:1965–1971. https://doi.org/10.1083/jcb.127.6.1965
34. Chrétien D, Fuller SD (2000) Microtubules switch occasionally into unfavorable configurations during elongation. J Mol Biol 298:663–676. https://doi.org/10.1006/jmbi.2000.3696
35. Manka SW, Moores CA (2018) Microtubule structure by cryo-EM: snapshots of dynamic instability. Essays Biochem 62:737–751. https://doi.org/10.1042/EBC20180031
36. Kuchnir Fygenson D, Flyvbjerg H, Sneppen K, et al (1995) Spontaneous nucleation of microtubules. Phys Rev E Stat Phys Plasmas Fluids Relat Interdiscip Top 51:5058–5063. https://doi.org/10.1103/physreve.51.5058
37. McIntosh JR, O'Toole E, Morgan G, et al (2018) Microtubules grow by the addition of bent guanosine triphosphate tubulin to the tips of curved protofilaments. J Cell Biol 217:2691–2708. https://doi.org/10.1083/jcb.201802138
38. Walker RA, O'Brien ET, Pryer NK, et al (1988) Dynamic instability of individual microtubules analyzed by video light microscopy: rate constants and transition frequencies. J Cell Biol 107:1437–1448. https://doi.org/10.1083/jcb.107.4.1437
39. Manka SW, Moores CA (2018) The role of tubulin–tubulin lattice contacts in the mechanism of microtubule dynamic instability. Nat Struct Mol Biol 25:607–615. https://doi.org/10.1038/s41594-018-0087-8
40. Howard J, Hyman AA (2009) Growth, fluctuation and switching at microtubule plus ends. Nat Rev Mol Cell Biol 10:569–574. https://doi.org/10.1038/nrm2713
41. Gardner MK, Zanic M, Howard J (2013) Microtubule catastrophe and rescue. Curr Opin Cell Biol 25:14–22. https://doi.org/10.1016/j.ceb.2012.09.006
42. Fourriere L, Jimenez AJ, Perez F, Boncompain G (2020) The role of microtubules in secretory protein transport. J Cell Sci 133:. https://doi.org/10.1242/jcs.237016
43. Maday S, Twelvetrees AE, Moughamian AJ, Holzbaur ELF (2014) Axonal Transport: Cargo-Specific Mechanisms of Motility and Regulation. Neuron 84:292–309. https://doi.org/10.1016/j.neuron.2014.10.019

44. Sleigh JN, Rossor AM, Fellows AD, et al (2019) Axonal transport and neurological disease. Nat Rev Neurol 15:691–703. https://doi.org/10.1038/s41582-019-0257-2
45. Prosser SL, Pelletier L (2017) Mitotic spindle assembly in animal cells: a fine balancing act. Nat Rev Mol Cell Biol 18:187–201. https://doi.org/10.1038/nrm.2016.162
46. Müller-Reichert T, Kiewisz R, Redemann S (2018) Mitotic spindles revisited – new insights from 3D electron microscopy. J Cell Sci 131:. https://doi.org/10.1242/jcs.211383
47. Lakshmi RB, Nair VM, Manna TK (2018) Regulators of spindle microtubules and their mechanisms: Living together matters. IUBMB Life 70:101–111. https://doi.org/10.1002/iub.1708
48. Vasiliev JM, Gelfand IM, Domnina LV, et al (1970) Effect of colcemid on the locomotory behaviour of fibroblasts. Development 24:625–640
49. Goldman RD (1971) The role of three cytoplasmic fibers in BHK-21 cell motility: I. Microtubules and the effects of colchicine. J Cell Biol 51:752–762. https://doi.org/10.1083/jcb.51.3.752
50. Ganguly A, Yang H, Sharma R, et al (2012) The Role of Microtubules and Their Dynamics in Cell Migration. J Biol Chem 287:43359–43369. https://doi.org/10.1074/jbc.M112.423905
51. Kopf A, Renkawitz J, Hauschild R, et al (2020) Microtubules control cellular shape and coherence in amoeboid migrating cells. J Cell Biol 219:. https://doi.org/10.1083/jcb.201907154
52. Khan S, Scholey JM (2018) Assembly, functions and evolution of archaella, flagella and cilia. Curr Biol 28:R278–R292. https://doi.org/10.1016/j.cub.2018.01.085
53. Bodakuntla S, Jijumon AS, Villablanca C, et al (2019) Microtubule-Associated Proteins: Structuring the Cytoskeleton. Trends Cell Biol 29:804–819. https://doi.org/10.1016/j.tcb.2019.07.004
54. Sanchez AD, Feldman JL (2017) Microtubule-organizing centers: from the centrosome to non-centrosomal sites. Curr Opin Cell Biol 44:93–101. https://doi.org/10.1016/j.ceb.2016.09.003
55. Wu J, Akhmanova A (2017) Microtubule-Organizing Centers. Annu Rev Cell Dev Biol 33:51–75. https://doi.org/10.1146/annurev-cellbio-100616-060615
56. Kollman JM, Merdes A, Mourey L, Agard DA (2011) Microtubule nucleation by γ-tubulin complexes. Nat Rev Mol Cell Biol 12:709–721. https://doi.org/10.1038/nrm3209
57. Tovey CA, Conduit PT (2018) Microtubule nucleation by γ-tubulin complexes and beyond. Essays Biochem 62:765–780. https://doi.org/10.1042/EBC20180028
58. Wiese C, Zheng Y (2000) A new function for the γ -tubulin ring complex as a microtubule minus-end cap. Nat Cell Biol 2:358–364. https://doi.org/10.1038/35014051
59. Mogensen MM, Malik A, Piel M, et al (2000) Microtubule minus-end anchorage at centrosomal and non-centrosomal sites: the role of ninein. J Cell Sci 113:3013–3023

60. Delgehyr N, Sillibourne J, Bornens M (2005) Microtubule nucleation and anchoring at the centrosome are independent processes linked by ninein function. J Cell Sci 118:1565–1575. https://doi.org/10.1242/jcs.02302
61. Al-Bassam J, Chang F (2011) Regulation of microtubule dynamics by TOG-domain proteins XMAP215/Dis1 and CLASP. Trends Cell Biol 21:604–614. https://doi.org/10.1016/j.tcb.2011.06.007
62. Nithianantham S, Cook BD, Beans M, et al (2018) Structural basis of tubulin recruitment and assembly by microtubule polymerases with tumor overexpressed gene (TOG) domain arrays. In: eLife. https://elifesciences.org/articles/38922/figures#figures-and-data. Accessed 7 Jan 2021
63. Bechstedt S, Brouhard GJ (2012) Doublecortin Recognizes the 13-Protofilament Microtubule Cooperatively and Tracks Microtubule Ends. Dev Cell 23:181–192. https://doi.org/10.1016/j.devcel.2012.05.006
64. Manka SW, Moores CA (2020) Pseudo-repeats in doublecortin make distinct mechanistic contributions to microtubule regulation. EMBO Rep 21:e51534. https://doi.org/10.15252/embr.202051534
65. Bechstedt S, Lu K, Brouhard GJ (2014) Doublecortin Recognizes the Longitudinal Curvature of the Microtubule End and Lattice. Curr Biol 24:2366–2375. https://doi.org/10.1016/j.cub.2014.08.039
66. Vitre B, Coquelle FM, Heichette C, et al (2008) EB1 regulates microtubule dynamics and tubulin sheet closure in vitro. Nat Cell Biol 10:415–421. https://doi.org/10.1038/ncb1703
67. Zhang R, LaFrance B, Nogales E (2018) Separating the effects of nucleotide and EB binding on microtubule structure. Proc Natl Acad Sci 115:E6191–E6200. https://doi.org/10.1073/pnas.1802637115
68. Pedersen LB, Geimer S, Sloboda RD, Rosenbaum JL (2003) The Microtubule Plus End-Tracking Protein EB1 Is Localized to the Flagellar Tip and Basal Bodies in Chlamydomonas reinhardtii. Curr Biol 13:1969–1974. https://doi.org/10.1016/j.cub.2003.10.058
69. Harris JA, Liu Y, Yang P, et al (2016) Single-particle imaging reveals intraflagellar transport–independent transport and accumulation of EB1 in *Chlamydomonas* flagella. Mol Biol Cell 27:295–307. https://doi.org/10.1091/mbc.e15-08-0608
70. Schroder JM, Larsen J, Komarova Y, et al (2011) EB1 and EB3 promote cilia biogenesis by several centrosome-related mechanisms. J Cell Sci 124:2539–2551. https://doi.org/10.1242/jcs.085852
71. Maurer SP, Fourniol FJ, Bohner G, et al (2012) EBs Recognize a Nucleotide-Dependent Structural Cap at Growing Microtubule Ends. Cell 149:371–382. https://doi.org/10.1016/j.cell.2012.02.049
72. Mallik R, Rai AK, Barak P, et al (2013) Teamwork in microtubule motors. Trends Cell Biol 23:575–582. https://doi.org/10.1016/j.tcb.2013.06.003
73. Nicastro D, Schwartz C, Pierson J, et al (2006) The molecular architecture of axonemes revealed by cryoelectron tomography. Science 313:944–948. https://doi.org/10.1126/science.1128618

74. Rao Q, Wang Y, Chai P, et al (2020) Cryo-EM structures of outer-arm dynein array bound to microtubule doublet reveal a mechanism for motor coordination. bioRxiv 44. https://doi.org/10.1101/2020.12.08.415687
75. Echandía ELR, Piezzi RS, Rodríguez EM (1968) Dense-core microtubules in neurons and gliocytes of the toad *Bufo arenarum* Hensel. Am J Anat 122:157–167. https://doi.org/10.1002/aja.1001220110
76. Burton PR (1984) Luminal material in microtubules of frog olfactory axons: structure and distribution. J Cell Biol 99:520–528. https://doi.org/10.1083/jcb.99.2.520
77. Xu Z, Afzelius BA (1988) The substructure of marginal bundles in human blood platelets. J Ultrastruct Mol Struct Res 99:244–253. https://doi.org/10.1016/0889-1605(88)90068-7
78. Garvalov BK, Zuber B, Bouchet-Marquis C, et al (2006) Luminal particles within cellular microtubules. J Cell Biol 174:759–765. https://doi.org/10.1083/jcb.200606074
79. Kar S, Fan J, Smith MJ, et al (2003) Repeat motifs of tau bind to the insides of microtubules in the absence of taxol. EMBO J 22:70–77. https://doi.org/10.1093/emboj/cdg001
80. Cuveillier C, Delaroche J, Seggio M, et al (2020) MAP6 is an intraluminal protein that induces neuronal microtubules to coil. Sci Adv 6:. https://doi.org/10.1126/sciadv.aaz4344
81. Paul DM, Mantell J, Borucu U, et al (2020) In situ cryo-electron tomography reveals filamentous actin within the microtubule lumen. J Cell Biol 219:. https://doi.org/10.1083/jcb.201911154
82. Kühlbrandt W (2014) The Resolution Revolution. Science 343:1443–1444. https://doi.org/10.1126/science.1251652
83. Nicastro D, Fu X, Heuser T, et al (2011) Cryo-electron tomography reveals conserved features of doublet microtubules in flagella. Proc Natl Acad Sci 108:E845–E853. https://doi.org/10.1073/pnas.1106178108
84. Ichikawa M, Liu D, Kastritis PL, et al (2017) Subnanometre-resolution structure of the doublet microtubule reveals new classes of microtubule-associated proteins. Nat Commun 8:15035. https://doi.org/10.1038/ncomms15035
85. Stoddard D, Zhao Y, Bayless BA, et al (2018) Tetrahymena RIB72A and RIB72B are microtubule inner proteins in the ciliary doublet microtubules. Mol Biol Cell 29:2566–2577. https://doi.org/10.1091/mbc.E18-06-0405
86. Owa M, Uchihashi T, Yanagisawa H, et al (2019) Inner lumen proteins stabilize doublet microtubules in cilia and flagella. Nat Commun 10:1143. https://doi.org/10.1038/s41467-019-09051-x
87. Ma M, Stoyanova M, Rademacher G, et al (2019) Structure of the Decorated Ciliary Doublet Microtubule. Cell 179:909-922.e12. https://doi.org/10.1016/j.cell.2019.09.030
88. Fabritius AS, Bayless BA, Li S, et al (2020) Proteomic analysis of microtubule inner proteins (MIPs) in Rib72 null Tetrahymena cells reveals functional MIPs. bioRxiv 2020.10.02.324467. https://doi.org/10.1101/2020.10.02.324467

89. Fisch C, Dupuis-Williams P (2011) Ultrastructure of cilia and flagella - back to the future! Biol Cell 103:249–270. https://doi.org/10.1042/BC20100139
90. Bayless BA, Navarro FM, Winey M (2019) Motile Cilia: Innovation and Insight From Ciliate Model Organisms. Front Cell Dev Biol 7:. https://doi.org/10.3389/fcell.2019.00265
91. Pearson CG, Winey M (2009) Basal Body Assembly in Ciliates: The Power of Numbers. Traffic 10:461–471. https://doi.org/10.1111/j.1600-0854.2009.00885.x
92. Greenan GA, Vale RD, Agard DA (2020) Electron cryotomography of intact motile cilia defines the basal body to axoneme transition. J Cell Biol 219:. https://doi.org/10.1083/jcb.201907060
93. Szymanska K, Johnson CA (2012) The transition zone: an essential functional compartment of cilia. Cilia 1:10. https://doi.org/10.1186/2046-2530-1-10
94. Reiter JF, Blacque OE, Leroux MR (2012) The base of the cilium: roles for transition fibres and the transition zone in ciliary formation, maintenance and compartmentalization. EMBO Rep 13:608–618. https://doi.org/10.1038/embor.2012.73
95. Dahl HA (1963) Fine structure of cilia in rat cerebral cortex. Z Für Zellforsch Mikrosk Anat 60:369–386. https://doi.org/10.1007/BF00336612
96. Wilsman NJ, Farnum CE, Reed-Aksamit DK (1980) Incidence and morphology of equine and murine chondrocytic cilia. Anat Rec 197:355–361. https://doi.org/10.1002/ar.1091970309
97. Gluenz E, Höög JL, Smith AE, et al (2010) Beyond 9+0: noncanonical axoneme structures characterize sensory cilia from protists to humans. FASEB J 24:3117–3121. https://doi.org/10.1096/fj.09-151381
98. Gui M, Ma M, Sze-Tu E, et al (2021) Structures of radial spokes and associated complexes important for ciliary motility. Nat Struct Mol Biol 28:29–37. https://doi.org/10.1038/s41594-020-00530-0
99. Yoshimura M, Shingyoji C (1999) Effects of the central pair apparatus on microtubule sliding velocity in sea urchin sperm flagella. Cell Struct Funct 24:43–54. https://doi.org/10.1247/csf.24.43
100. Nakano I, Kobayashi T, Yoshimura M, Shingyoji C (2003) Central-pair-linked regulation of microtubule sliding by calcium in flagellar axonemes. J Cell Sci 116:1627–1636. https://doi.org/10.1242/jcs.00336
101. Lin J, Okada K, Raytchev M, et al (2014) Structural mechanism of the dynein power stroke. Nat Cell Biol 16:479–485. https://doi.org/10.1038/ncb2939
102. Odor DL, Blandau RJ (1985) Observations on the solitary cilium of rabbit oviductal epithelium: Its motility and ultrastructure. Am J Anat 174:437–453. https://doi.org/10.1002/aja.1001740407
103. Nonaka S, Tanaka Y, Okada Y, et al (1998) Randomization of Left–Right Asymmetry due to Loss of Nodal Cilia Generating Leftward Flow of Extraembryonic Fluid in Mice Lacking KIF3B Motor Protein. Cell 95:829–837. https://doi.org/10.1016/S0092-8674(00)81705-5

104. Woolley DM, Nickels SN (1985) Microtubule termination patterns in mammalian sperm flagella. J Ultrastruct Res 90:221–234. https://doi.org/10.1016/S0022-5320(85)80001-0
105. Rogowski M, Scholz D, Geimer S (2013) Electron microscopy of flagella, primary cilia, and intraflagellar transport in flat-embedded cells. Methods Enzymol 524:243–263. https://doi.org/10.1016/B978-0-12-397945-2.00014-7
106. Louka P, Vasudevan KK, Guha M, et al (2018) Proteins that control the geometry of microtubules at the ends of cilia. J Cell Biol 217:4298–4313. https://doi.org/10.1083/jcb.201804141
107. Croft JT, Zabeo D, Subramanian R, Höög JL (2018) Composition, structure and function of the eukaryotic flagellum distal tip. Essays Biochem 62:815–828. https://doi.org/10.1042/EBC20180032
108. Moran DT, Rowley JC, Jafek BW, Lovell MA (1982) The fine structure of the olfactory mucosa in man. J Neurocytol 11:721–746. https://doi.org/10.1007/BF01153516
109. Doroquez DB, Berciu C, Anderson JR, et al (2014) A high-resolution morphological and ultrastructural map of anterior sensory cilia and glia in Caenorhabditis elegans. eLife 3:e01948. https://doi.org/10.7554/eLife.01948
110. Gilliam JC, Chang JT, Sandoval IM, et al (2012) Three-Dimensional Architecture of the Rod Sensory Cilium and Its Disruption in Retinal Neurodegeneration. Cell 151:1029–1041. https://doi.org/10.1016/j.cell.2012.10.038
111. Downing KH, Sui H (2007) Structural insights into microtubule doublet interactions in axonemes. Curr Opin Struct Biol 17:253–259. https://doi.org/10.1016/j.sbi.2007.03.013
112. Gadelha C, Wickstead B, Gull K (2007) Flagellar and ciliary beating in trypanosome motility. Cell Motil 64:629–643. https://doi.org/10.1002/cm.20210
113. Silflow CD, Lefebvre PA (2001) Assembly and motility of eukaryotic cilia and flagella. Lessons from *Chlamydomonas reinhardtii*. Plant Physiol 127:1500–1507. https://doi.org/10.1104/pp.010807
114. Witman GB (1993) *Chlamydomonas* phototaxis. Trends Cell Biol 3:403–408. https://doi.org/10.1016/0962-8924(93)90091-E
115. Fahy JV, Dickey BF (2010) Airway mucus function and dysfunction. N Engl J Med 363:2233–2247. https://doi.org/10.1056/NEJMra0910061
116. Ramirez-San Juan GR, Mathijssen AJTM, He M, et al (2020) Multi-scale spatial heterogeneity enhances particle clearance in airway ciliary arrays. Nat Phys 16:958–964. https://doi.org/10.1038/s41567-020-0923-8
117. O'Callaghan CL, Sikand K, Rutman A, Hirst RA (2008) The effect of viscous loading on brain ependymal cilia. Neurosci Lett 439:56–60. https://doi.org/10.1016/j.neulet.2008.04.095
118. Singla V, Reiter JF (2006) The primary cilium as the cell's antenna: signaling at a sensory organelle. Science 313:629–633. https://doi.org/10.1126/science.1124534

119. Hilgendorf KI, Johnson CT, Jackson PK (2016) The primary cilium as a cellular receiver: organizing ciliary GPCR signaling. Curr Opin Cell Biol 39:84–92. https://doi.org/10.1016/j.ceb.2016.02.008
120. Bloodgood RA (2010) Sensory reception is an attribute of both primary cilia and motile cilia. J Cell Sci 123:505–509. https://doi.org/10.1242/jcs.066308
121. Shah AS, Ben-Shahar Y, Moninger TO, et al (2009) Motile cilia of human airway epithelia are chemosensory. Science 325:1131–1134. https://doi.org/10.1126/science.1173869
122. Wheway G, Nazlamova L, Hancock JT (2018) Signaling through the Primary Cilium. Front Cell Dev Biol 6:. https://doi.org/10.3389/fcell.2018.00008
123. Briscoe J, Thérond PP (2013) The mechanisms of Hedgehog signalling and its roles in development and disease. Nat Rev Mol Cell Biol 14:416–429. https://doi.org/10.1038/nrm3598
124. Subota I, Julkowska D, Vincensini L, et al (2014) Proteomic analysis of intact flagella of procyclic *Trypanosoma brucei* cells identifies novel flagellar proteins with unique sub-localization and dynamics. Mol Cell Proteomics 13:1769–1786. https://doi.org/10.1074/mcp.M113.033357
125. Pazour GJ, Agrin N, Leszyk J, Witman GB (2005) Proteomic analysis of a eukaryotic cilium. J Cell Biol 170:103–113. https://doi.org/10.1083/jcb.200504008
126. Mayer U, Küller A, Daiber PC, et al (2009) The proteome of rat olfactory sensory cilia. PROTEOMICS 9:322–334. https://doi.org/10.1002/pmic.200800149
127. Ishikawa H, Thompson J, Yates JR, Marshall WF (2012) Proteomic Analysis of Mammalian Primary Cilia. Curr Biol 22:414–419. https://doi.org/10.1016/j.cub.2012.01.031
128. Putoux A, Thomas S, Coene KLM, et al (2011) KIF7 mutations cause fetal hydrolethalus and acrocallosal syndromes. Nat Genet 43:601–606. https://doi.org/10.1038/ng.826
129. Amiri-Yekta A, Coutton C, Kherraf Z-E, et al (2016) Whole-exome sequencing of familial cases of multiple morphological abnormalities of the sperm flagella (MMAF) reveals new DNAH1 mutations. Hum Reprod 31:2872–2880. https://doi.org/10.1093/humrep/dew262
130. Tang S, Wang X, Li W, et al (2017) Biallelic Mutations in CFAP43 and CFAP44 Cause Male Infertility with Multiple Morphological Abnormalities of the Sperm Flagella. Am J Hum Genet 100:854–864. https://doi.org/10.1016/j.ajhg.2017.04.012
131. Wang X, Jin H, Han F, et al (2017) Homozygous DNAH1 frameshift mutation causes multiple morphological anomalies of the sperm flagella in Chinese. Clin Genet 91:313–321. https://doi.org/10.1111/cge.12857
132. Coutton C, Vargas AS, Amiri-Yekta A, et al (2018) Mutations in CFAP43 and CFAP44 cause male infertility and flagellum defects in Trypanosoma and human. Nat Commun 9:686. https://doi.org/10.1038/s41467-017-02792-7

133. Reiter JF, Leroux MR (2017) Genes and molecular pathways underpinning ciliopathies. Nat Rev Mol Cell Biol 18:533–547. https://doi.org/10.1038/nrm.2017.60
134. Afzelius B (1976) A human syndrome caused by immotile cilia. Science 193:317–319. https://doi.org/10.1126/science.1084576
135. Praveen K, Davis EE, Katsanis N (2015) Unique among ciliopathies: primary ciliary dyskinesia, a motile cilia disorder. F1000prime Rep 7:36. https://doi.org/10.12703/P7-36
136. Wallmeier J, Nielsen KG, Kuehni CE, et al (2020) Motile ciliopathies. Nat Rev Dis Primer 6:1–29. https://doi.org/10.1038/s41572-020-0209-6
137. Allen C, Borisy GG (1974) Structural polarity and directional growth of microtubules of Chlamydomonas flagella. J Mol Biol 90:381–402. https://doi.org/10.1016/0022-2836(74)90381-7
138. Höög JL, Lacomble S, O'Toole ET, et al (2014) Modes of flagellar assembly in *Chlamydomonas reinhardtii* and *Trypanosoma brucei*. eLife 3:e01479. https://doi.org/10.7554/eLife.01479
139. Marshall WF, Rosenbaum JL (2001) Intraflagellar transport balances continuous turnover of outer doublet microtubules: implications for flagellar length control. J Cell Biol 155:405–414. https://doi.org/10.1083/jcb.200106141
140. Kozminski KG, Johnson KA, Forscher P, Rosenbaum JL (1993) A motility in the eukaryotic flagellum unrelated to flagellar beating. Proc Natl Acad Sci U S A 90:5519–5523. https://doi.org/10.1073/pnas.90.12.5519
141. Jordan MA, Diener DR, Stepanek L, Pigino G (2018) The cryo-EM structure of intraflagellar transport trains reveals how dynein is inactivated to ensure unidirectional anterograde movement in cilia. Nat Cell Biol 20:1250–1255. https://doi.org/10.1038/s41556-018-0213-1
142. Nakane T, Kotecha A, Sente A, et al (2020) Single-particle cryo-EM at atomic resolution. Nature 587:152–156. https://doi.org/10.1038/s41586-020-2829-0
143. Yip KM, Fischer N, Paknia E, et al (2020) Atomic-resolution protein structure determination by cryo-EM. Nature 587:157–161. https://doi.org/10.1038/s41586-020-2833-4
144. Hayat MA (2000) Principles and Techniques of Electron Microscopy: Biological Applications. Cambridge University Press
145. Baker LA, Smith EA, Bueler SA, Rubinstein JL (2010) The resolution dependence of optimal exposures in liquid nitrogen temperature electron cryomicroscopy of catalase crystals. J Struct Biol 169:431–437. https://doi.org/10.1016/j.jsb.2009.11.014
146. Ellis EA, Cohen-Gould L (2016) Recognizing and Preventing Artifacts in Microscopy: A Roundtable Discussion. Microsc Microanal 22:2074–2075. https://doi.org/10.1017/S1431927616011211
147. Mielańczyk Ł, Matysiak N, Wojnicz OK and R (2015) Transmission Electron Microscopy of Biological Samples. Transm Electron Microsc - Theory Appl. https://doi.org/10.5772/60680

148. Winey M, Meehl JB, O'Toole ET, Giddings TH (2014) Conventional transmission electron microscopy. Mol Biol Cell 25:319–323. https://doi.org/10.1091/mbc.e12-12-0863
149. Scarff CA, Fuller MJG, Thompson RF, Iadaza MG (2018) Variations on Negative Stain Electron Microscopy Methods: Tools for Tackling Challenging Systems. JoVE J Vis Exp e57199. https://doi.org/10.3791/57199
150. Barreto-Vieira DF, Barth OM (2015) Negative and Positive Staining in Transmission Electron Microscopy for Virus Diagnosis. Microbiol Agric Hum Health. https://doi.org/10.5772/60511
151. Harris R, Bhella D, Adrian M (2006) Recent developments in negative staining for transmission electron microscopy. Microsc Anal 113:17
152. Harris JR, De Carlo S (2014) Negative Staining and Cryo-negative Staining: Applications in Biology and Medicine. In: Kuo J (ed) Electron Microscopy: Methods and Protocols. Humana Press, Totowa, NJ, pp 215–258
153. Giddings TH, O'Toole ET, Morphew M, et al (2001) Using rapid freeze and freeze-substitution for the preparation of yeast cells for electron microscopy and three-dimensional analysis. In: Methods in Cell Biology. Academic Press, pp 27–42
154. McDonald KL, Sharp DJ, Rickoll W (2012) Preparation of Drosophila specimens for examination by transmission electron microscopy. Cold Spring Harb Protoc 2012:1044–1048. https://doi.org/10.1101/pdb.top068452
155. McDonald K, Schwarz H, Müller-Reichert T, et al (2010) Chapter 28 - "Tips and Tricks" for High-Pressure Freezing of Model Systems. In: Müller-Reichert T (ed) Methods in Cell Biology. Academic Press, pp 671–693
156. Höög JL, Gluenz E, Vaughan S, Gull K (2010) Chapter 8 - Ultrastructural Investigation Methods for Trypanosoma brucei. In: Müller-Reichert T (ed) Methods in Cell Biology. Academic Press, pp 175–196
157. Reynolds ES (1963) The use of lead citrate at high pH as an electron-opaque stain in electron microscopy. J Cell Biol 17:208–212. https://doi.org/10.1083/jcb.17.1.208
158. Thompson RF, Walker M, Siebert CA, et al (2016) An introduction to sample preparation and imaging by cryo-electron microscopy for structural biology. Methods 100:3–15. https://doi.org/10.1016/j.ymeth.2016.02.017
159. Shen PS (2018) The 2017 Nobel Prize in Chemistry: cryo-EM comes of age. Anal Bioanal Chem 410:2053–2057. https://doi.org/10.1007/s00216-018-0899-8
160. Dubochet J, McDowall AW (1981) Vitrification of pure water for electron microscopy. J Microsc 124:3–4. https://doi.org/10.1111/j.1365-2818.1981.tb02483.x
161. Dubochet J, Adrian M, Chang J-J, et al (1988) Cryo-electron microscopy of vitrified specimens. Q Rev Biophys 21:129–228. https://doi.org/10.1017/S0033583500004297

162. Song YS, Adler D, Xu F, et al (2010) Vitrification and levitation of a liquid droplet on liquid nitrogen. Proc Natl Acad Sci 107:4596–4600. https://doi.org/10.1073/pnas.0914059107
163. Dobro MJ, Melanson LA, Jensen GJ, McDowall AW (2010) Chapter Three - Plunge Freezing for Electron Cryomicroscopy. In: Jensen GJ (ed) Methods in Enzymology. Academic Press, pp 63–82
164. O'Toole ET, Winey M, McIntosh JR, Mastronarde DN (2002) Electron tomography of yeast cells. In: Methods in Enzymology. Academic Press, pp 81–96
165. Lučić V, Förster F, Baumeister W (2005) Structural studies by electron tomography: from cells to molecules. Annu Rev Biochem 74:833–865. https://doi.org/10.1146/annurev.biochem.73.011303.074112
166. Castaño-Díez D, Kudryashev M, Arheit M, Stahlberg H (2012) Dynamo: A flexible, user-friendly development tool for subtomogram averaging of cryo-EM data in high-performance computing environments. J Struct Biol 178:139–151. https://doi.org/10.1016/j.jsb.2011.12.017
167. Bharat TAM, Scheres SHW (2016) Resolving macromolecular structures from electron cryo-tomography data using subtomogram averaging in RELION. Nat Protoc 11:2054–2065. https://doi.org/10.1038/nprot.2016.124
168. Kremer JR, Mastronarde DN, McIntosh JR (1996) Computer visualization of three-dimensional image data using IMOD. J Struct Biol 116:71–76. https://doi.org/10.1006/jsbi.1996.0013
169. Scheres SHW (2012) RELION: Implementation of a Bayesian approach to cryo-EM structure determination. J Struct Biol 180:519–530. https://doi.org/10.1016/j.jsb.2012.09.006
170. Sigworth FJ (2016) Principles of cryo-EM single-particle image processing. Microscopy 65:57–67. https://doi.org/10.1093/jmicro/dfv370
171. Song K, Shang Z, Fu X, et al (2020) In situ structure determination at nanometer resolution using TYGRESS. Nat Methods 17:201–208. https://doi.org/10.1038/s41592-019-0651-0
172. Grant T, Rohou A, Grigorieff N (2018) cisTEM, user-friendly software for single-particle image processing. eLife 7:e35383. https://doi.org/10.7554/eLife.35383
173. Guraya SS (1987) Biology of Spermatogenesis and Spermatozoa in Mammals, 1st ed. Springer-Verlag Berlin Heidelberg
174. Gu N-H, Zhao W-L, Wang G-S, Sun F (2019) Comparative analysis of mammalian sperm ultrastructure reveals relationships between sperm morphology, mitochondrial functions and motility. Reprod Biol Endocrinol 17:66. https://doi.org/10.1186/s12958-019-0510-y
175. Fawcett DW (1975) The mammalian spermatozoon. Dev Biol 44:394–436. https://doi.org/10.1016/0012-1606(75)90411-X
176. Cummins JM, Woodall PF (1985) On mammalian sperm dimensions. Reproduction 75:153–175. https://doi.org/10.1530/jrf.0.0750153
177. Steven Ward W, Coffey DS (1991) DNA Packaging and Organization in Mammalian Spermatozoa: Comparison with Somatic Cell. Biol Reprod 44:569–574. https://doi.org/10.1095/biolreprod44.4.569

178. Miller D, Brinkworth M, Iles D (2010) Paternal DNA packaging in spermatozoa: more than the sum of its parts? DNA, histones, protamines and epigenetics. Reproduction 139:287–301. https://doi.org/10.1530/REP-09-0281
179. Balhorn R (2007) The protamine family of sperm nuclear proteins. Genome Biol 8:227. https://doi.org/10.1186/gb-2007-8-9-227
180. Austin CR, Bishop MWH, Parkes AS (1958) Role of the rodent acrosome and perforatorium in fertilization. Proc R Soc Lond Ser B - Biol Sci 149:241–248. https://doi.org/10.1098/rspb.1958.0066
181. Berruti G, Paiardi C (2011) Acrosome biogenesis. Spermatogenesis 1:95–98. https://doi.org/10.4161/spmg.1.2.16820
182. Ounjai P, Kim KD, Lishko PV, Downing KH (2012) Three-Dimensional Structure of the Bovine Sperm Connecting Piece Revealed by Electron Cryotomography. Biol Reprod 87:. https://doi.org/10.1095/biolreprod.112.101980
183. Woolley DM, Carter DA, Tilly GN (2008) Compliance in the neck structures of the guinea pig spermatozoon, as indicated by rapid freezing and electron microscopy. J Anat 213:336–341. https://doi.org/10.1111/j.1469-7580.2008.00919.x
184. Manandhar G, Simerly C, Schatten G (2000) Highly degenerated distal centrioles in rhesus and human spermatozoa. Hum Reprod 15:256–263. https://doi.org/10.1093/humrep/15.2.256
185. Ruiz-Pesini E, Díez-Sánchez C, López-Pérez MJ, Enríquez JA (2007) The Role of the Mitochondrion in Sperm Function: Is There a Place for Oxidative Phosphorylation or Is This a Purely Glycolytic Process? In: Current Topics in Developmental Biology. Academic Press, pp 3–19
186. Storey BT (2004) Mammalian sperm metabolism: oxygen and sugar, friend and foe. Int J Dev Biol 52:427–437. https://doi.org/10.1387/ijdb.072522bs
187. Ho H-C, Wey S (2007) Three dimensional rendering of the mitochondrial sheath morphogenesis during mouse spermiogenesis. Microsc Res Tech 70:719–723. https://doi.org/10.1002/jemt.20457
188. Phillips DM (1977) Mitochondrial disposition in mammalian spermatozoa. J Ultrastruct Res 58:144–154. https://doi.org/10.1016/S0022-5320(77)90026-0
189. Olson GE, Sammons DW (1980) Structural chemistry of outer dense fibers of rat sperm. Biol Reprod 22:319–332. https://doi.org/10.1095/biolreprod22.2.319
190. Baltz JM, Oneeka Williams P, Cone RA (1990) Dense fibers protect mammalian sperm against damage. Biol Reprod 43:485–491. https://doi.org/10.1095/biolreprod43.3.485
191. Zhao W, Li Z, Ping P, et al (2018) Outer dense fibers stabilize the axoneme to maintain sperm motility. J Cell Mol Med 22:1755–1768. https://doi.org/10.1111/jcmm.13457
192. Lindemann CB, Lesich KA (2016) Functional anatomy of the mammalian sperm flagellum. Cytoskeleton 73:652–669. https://doi.org/10.1002/cm.21338

193. Serres C, Escalier D, David G (1983) Ultrastructural morphometry of the human sperm flagellum with a stereological analysis of the lengths of the dense fibres. Biol Cell 49:153–161
194. Eddy EM, Toshimori K, O'Brien DA (2003) Fibrous sheath of mammalian spermatozoa. Microsc Res Tech 61:103–115. https://doi.org/10.1002/jemt.10320
195. Gadêlha H, Hernández-Herrera P, Montoya F, et al (2020) Human sperm uses asymmetric and anisotropic flagellar controls to regulate swimming symmetry and cell steering. Sci Adv 6:eaba5168. https://doi.org/10.1126/sciadv.aba5168
196. Neal CV, Hall-McNair AL, Kirkman-Brown J, et al (2020) Doing more with less: The flagellar end piece enhances the propulsive effectiveness of human spermatozoa. Phys Rev Fluids 5:073101. https://doi.org/10.1103/PhysRevFluids.5.073101
197. Ringo DL (1967) Flagellar motion and fine structure of the flagellar apparatus in *Chlamydomonas*. J Cell Biol 33:543–571. https://doi.org/10.1083/jcb.33.3.543
198. Satish Tammana TV, Tammana D, Diener DR, Rosenbaum J (2013) Centrosomal protein CEP104 (*Chlamydomonas* FAP256) moves to the ciliary tip during ciliary assembly. J Cell Sci 126:5018–5029. https://doi.org/10.1242/jcs.133439
199. Reynolds MJ, Phetruen T, Fisher RL, et al (2018) The developmental process of the growing motile ciliary tip region. Sci Rep 8:7977. https://doi.org/10.1038/s41598-018-26111-2
200. Woolley D, Gadelha C, Gull K (2006) Evidence for a sliding-resistance at the tip of the trypanosome flagellum. Cell Motil 63:741–746. https://doi.org/10.1002/cm.20159
201. O'Hagan R, Piasecki BP, Silva M, et al (2011) The tubulin deglutamylase CCPP-1 regulates the function and stability of sensory cilia in *C. elegans*. Curr Biol 21:1685–1694. https://doi.org/10.1016/j.cub.2011.08.049
202. O'Hagan R, Silva M, Nguyen KCQ, et al (2017) Glutamylation regulates transport, specializes function, and sculpts the structure of cilia. Curr Biol 27:3430-3441.e6. https://doi.org/10.1016/j.cub.2017.09.066
203. Silva M, Morsci N, Nguyen KCQ, et al (2017) Cell-specific α-tubulin isotype regulates ciliary microtubule ultrastructure, intraflagellar transport, and extracellular vesicle biology. Curr Biol 27:968–980. https://doi.org/10.1016/j.cub.2017.02.039
204. Berrueta L, Kraeft S-K, Tirnauer JS, et al (1998) The adenomatous polyposis coli-binding protein EB1 is associated with cytoplasmic and spindle microtubules. Proc Natl Acad Sci 95:10596–10601. https://doi.org/10.1073/pnas.95.18.10596
205. Howes SC, Geyer EA, LaFrance B, et al (2018) Structural and functional differences between porcine brain and budding yeast microtubules. Cell Cycle 17:278–287. https://doi.org/10.1080/15384101.2017.1415680
206. Maheshwari A, Obbineni JM, Bui KH, et al (2015) α- and β-Tubulin Lattice of the Axonemal Microtubule Doublet and Binding Proteins

Revealed by Single Particle Cryo-Electron Microscopy and Tomography. Structure 23:1584–1595. https://doi.org/10.1016/j.str.2015.06.017
207. San Agustin JT, Pazour GJ, Witman GB (2015) Intraflagellar transport is essential for mammalian spermiogenesis but is absent in mature sperm. Mol Biol Cell 26:4358–4372. https://doi.org/10.1091/mbc.e15-08-0578
208. Riedel-Kruse IH, Hilfinger A, Howard J, Jülicher F (2007) How molecular motors shape the flagellar beat. HFSP J 1:192–208. https://doi.org/10.2976/1.2773861
209. Saggiorato G, Alvarez L, Jikeli JF, et al (2017) Human sperm steer with second harmonics of the flagellar beat. Nat Commun 8:1415. https://doi.org/10.1038/s41467-017-01462-y
210. Ho C-M, Li X, Lai M, et al (2020) Bottom-up structural proteomics: cryoEM of protein complexes enriched from the cellular milieu. Nat Methods 17:79–85. https://doi.org/10.1038/s41592-019-0637-y
211. Martínez-Heredia J, Estanyol JM, Ballescà JL, Oliva R (2006) Proteomic identification of human sperm proteins. PROTEOMICS 6:4356–4369. https://doi.org/10.1002/pmic.200600094
212. Baker MA, Reeves G, Hetherington L, et al (2007) Identification of gene products present in Triton X-100 soluble and insoluble fractions of human spermatozoa lysates using LC-MS/MS analysis. PROTEOMICS – Clin Appl 1:524–532. https://doi.org/10.1002/prca.200601013
213. Amaral A, Castillo J, Estanyol JM, et al (2013) Human Sperm Tail Proteome Suggests New Endogenous Metabolic Pathways. Mol Cell Proteomics 12:330–342. https://doi.org/10.1074/mcp.M112.020552
214. Baker MA, Naumovski N, Hetherington L, et al (2013) Head and flagella subcompartmental proteomic analysis of human spermatozoa. PROTEOMICS 13:61–74. https://doi.org/10.1002/pmic.201200350
215. Wang G, Guo Y, Zhou T, et al (2013) In-depth proteomic analysis of the human sperm reveals complex protein compositions. J Proteomics 79:114–122. https://doi.org/10.1016/j.jprot.2012.12.008
216. Jumeau F, Com E, Lane L, et al (2015) Human Spermatozoa as a Model for Detecting Missing Proteins in the Context of the Chromosome-Centric Human Proteome Project. J Proteome Res 14:3606–3620. https://doi.org/10.1021/acs.jproteome.5b00170
217. Varga V, Moreira-Leite F, Portman N, Gull K (2017) Protein diversity in discrete structures at the distal tip of the trypanosome flagellum. Proc Natl Acad Sci 114:E6546–E6555. https://doi.org/10.1073/pnas.1703553114
218. Pihlaja DJ, Roth LE, Consigli RA (1973) Bovine Sperm Fractionation: I. Selective Degradation and Segment Separation1. Biol Reprod 8:311–320. https://doi.org/10.1093/biolreprod/8.3.311
219. Wyatt Shields IV C, Reyes CD, López GP (2015) Microfluidic cell sorting: a review of the advances in the separation of cells from debulking to rare cell isolation. Lab Chip 15:1230–1249. https://doi.org/10.1039/C4LC01246A
220. Jumeau F, Chalmel F, Fernandez-Gomez F-J, et al (2017) Defining the human sperm microtubulome: an integrated genomics approach. Biol Reprod 96:93–106. https://doi.org/10.1095/biolreprod.116.143479

221. Glish GL, Vachet RW (2003) The basics of mass spectrometry in the twenty-first century. Nat Rev Drug Discov 2:140–150. https://doi.org/10.1038/nrd1011
222. Zubarev RA, Makarov A (2013) Orbitrap Mass Spectrometry. Anal Chem 85:5288–5296. https://doi.org/10.1021/ac4001223
223. Dayon L, Hainard A, Licker V, et al (2008) Relative Quantification of Proteins in Human Cerebrospinal Fluids by MS/MS Using 6-Plex Isobaric Tags. Anal Chem 80:2921–2931. https://doi.org/10.1021/ac702422x
224. Altschul SF, Gish W, Miller W, et al (1990) Basic local alignment search tool. J Mol Biol 215:403–410. https://doi.org/10.1016/S0022-2836(05)80360-2
225. Fish KN (2009) Total Internal Reflection Fluorescence (TIRF) Microscopy. Curr Protoc Cytom 50:12.18.1-12.18.13. https://doi.org/10.1002/0471142956.cy1218s50
226. Shah NB, Duncan TM (2014) Bio-layer Interferometry for Measuring Kinetics of Protein-protein Interactions and Allosteric Ligand Effects. JoVE J Vis Exp e51383. https://doi.org/10.3791/51383
227. Burger D, Stihle M, Sharma A, et al (2016) Crystal Structures of the Human Doublecortin C- and N-terminal Domains in Complex with Specific Antibodies*. J Biol Chem 291:16292–16306. https://doi.org/10.1074/jbc.M116.726547